STUDY ON THE PARTICLE NATURE OF DARK MATTER

by

Manuel Fernando Sánchez Alarcón

A dissertation submitted in partial satisfaction of the requirements for the degree of
Bachelor

in

Physics

at

Universidad de los Andes

Adviser: Andrés Flórez

Bogotá, Colombia.

November 29, 2018

Dedicado a:

Mi madre, por enseñarme a seguir adelante a pesar de todo.
Mi hermano, por cuidarme y ser uno de los que me ha impulsado a seguir este camino. Le debo mi vida.
Mi hermana, por ser una compañía en medio de la adversidad.
Ewig dein, ewig mein, ewig uns.

Agradecimientos:

Agradezco a mi asesor, por poner su confianza en mi para la realización de este trabajo. También agradezco a todos y todo lo que me ha permitido llegar hasta este punto en mi vida.

Contents

List of Figures

Chapter 1

INTRODUCTION

Physics has tried to explain the how and why of the observable phenomena of nature since its inception. Some branches of physics have been remarkable for their predictions: Newtonian Mechanics, General Relativity, Quantum Mechanics, among others. These branches have allowed to understand many properties of the so called baryonic matter, which is believed to represent only roughly 5% of the total energy content of the universe. Some modern theories propose that the remaining 95% of the universe consist of Dark Matter (DM) and Dark Energy [1], of which not much is known yet. The eventual discovery and understanding of dark matter and dark energy, imply a complete understanding of the basic composition of the universe, answering one of the most profound questions in science today.

Dark matter does not interact electromagnetically [2], making it very difficult to be detected through direct measurement experiments. There are indirect ways to make measurements of variables associated with Dark Matter: Dynamics of galaxy clusters, gravitational lenses, detection of annihilation signals of WIMPs, among others [3]. With these observations, some models can be proposed, based in the known physics, to predict the general properties of this type of matter. Furthermore, understanding the particle nature of dark matter is the only way to accurately determine the actual dark matter relic density in the universe, responsible for the structure of planetary systems and galaxies.

In order to understand some of the properties of Dark Matter, it is nec-

essary to resort to particle physics and computational simulations. Particle physics can account for the microscopic nature of Dark Matter [4], while computational simulations can emulate its macroscopic behavior.

Through computational simulations of the movement of stars or the structure of galaxies, only some concepts about dark matter can be understood. For a complete understanding of this subject, it is necessary to study the particle nature of dark matter. The present document aims to deepen into the fundamental concepts about the relic dark matter density from the perspective of particle physics.

Chapter 2

OBJECTIVES

2.1 General Objective

Perform a study about the collisional terms in the Boltzmann equation to explain the relic DM density in the universe.

2.2 Specific Objectives

(a) Understand the annihilation cross section implicit in the DM relic density calculation.

(b) Develop a simulation to predict the density of a DM halo including collisional terms.

(c) Compare existing results for the DM relic density with the results considering collisional terms.

Chapter 3

METHODOLOGY

This work have a theoretical and computational approach, both are equally important. The theoretical work is done reviewing existing literature about the cosmological properties of Dark Matter and its particle nature, performing all the necessary calculations to reproduce and, if possible, extent the results to make them more comprehensive to the general public. The computational simulations are performed using C++ implementing the Lattice-Boltzmann Method for a certain number of particles in a two dimensional space or, if possible, three dimensional space that have a probability of colliding and others of being scattered. A graphical analysis of the results of the simulation is done using the software ROOT. The results of the simulation are compared with the theoretical predictions in the first part of this document with the aim of supporting the theory developed in the first chapters.

Chapter 4

STATE OF THE ART

4.1 A Brief Review of the Standard Model of Particle Physics

4.1.1 Astrophysical Distribution of Dark Matter

In order to seek DM effects in galaxies is necessary a "DM tracer", something that could show the effects of this type of matter without any other interference with baryonic matter. Stars can be used as DM tracers because the time between collisions with other stars is $\sim 10^{21}$ years.

We can deduct that, if a star does not collide with others in a very long time, only gravitational interactions can dictate their motion. From Newtonian physics we can derive the expression for the circular velocity of stars v_c, in the limit when the acceleration associated with the gravitational force is equal to the radial acceleration, related with the motion of stars in the galactic disk. A explicit form of v_c is shown in (4.1):

$$\begin{aligned} \frac{v_c^2}{r} &= \frac{GM}{r^2} \\ v_c &= \sqrt{\frac{GM}{r}}, \end{aligned} \tag{4.1}$$

where M is the enclosed mass (mass in the galactic disk), r is the distance from the center of the galaxy to another point, and G is the gravitational

constant. Observations show that the velocity remains constant at distances greater than the radius of the galactic disk, indicating that $M \propto r$ in this range, in other words, there is matter that can not be seen in these points of space. This type of matter described before is called Dark Matter. A expression for the density distribution of DM is presented in Equation (4.2):

$$\begin{aligned} \rho &= \frac{M_{halo}}{\frac{4}{3}\pi r^3} \\ &\sim \frac{r}{r^3} \\ &\sim \frac{1}{r^2}, \end{aligned} \tag{4.2}$$

if we assume DM is distributed as a spherically symmetric halo about the center of the galaxy. In Equation (4.2) M_{halo} is the mass of the DM halo. With the assumption that the DM halo is spherically symmetric it is possible to deduce a relation to find M_{halo}, from the definition of mass density:

$$\begin{aligned} dM_{halo} &= 4\pi r^2 \rho \, dr \\ M_{Halo} &= \int_0^{R_{Halo}} 4\pi r^2 \rho \, dr \\ &\sim R_{Halo}\rho_0, \end{aligned} \tag{4.3}$$

where ρ_0 is a constant such that $\rho = \frac{\rho_0}{r^2}$ and R_{halo} is the radius of the DM halo. In the Milky Way the total mass of the halo is $M_{Halo} \sim 10^{12} M_\odot \sim 10^{42} kg$ and $\rho_0 \sim 0.3 GeV/cm^3 \sim 4.8 \times 10^{-17} J/m^3$ [4], resulting in $R_{Halo} \sim 100\, Kpc$. In astronomy, the mass of the sun, $1.989 \times 10^{30}\, Kg$, is represented through $M_\odot$.

Using the virial theorem [5] a expression for the mean velocity of the DM halo can be deduced as shown in Equation (4.4):

$$\begin{aligned} \langle T \rangle &= -\frac{1}{2} \langle V \rangle \\ \left\langle \frac{1}{2} m v^2 \right\rangle &= -\frac{1}{2} \left\langle -\frac{GMm}{r} \right\rangle \\ \langle v^2 \rangle &= G \left\langle \frac{M}{r} \right\rangle \\ &\sim G \frac{M_{Halo}}{R_{Halo}} \\ \langle v \rangle &\sim 200\, km/s. \end{aligned} \tag{4.4}$$

It is important to note that so far DM has been considered to be non-relativistic and collisionless (all of the calculations above use non-relativistic arguments) which guide us to say that velocity and density distribution are related through only gravitational interactions. To analyze the dynamics of the DM halo, assuming that it does not collide with any external body, it is necessary to talk about the Boltzmann equation and the Jeans theorem, which is presented next.

4.1.2 Boltzmann Equation and Jeans Theorem

The Boltzmann equation describes the evolution of the phase-space density $f(\mathbf{x}, \mathbf{v})$ through time, where $\mathbf{x}$ is the position and $\mathbf{v}$ the velocity. The expression $f(\mathbf{x}, \mathbf{v}) d^3\mathbf{x} d^3\mathbf{v}$ is the probability of finding the particle in some volume in phase-space. The fact that the probability is preserved is expressed in Equation (4.5):

$$\int f(\mathbf{x}, \mathbf{v}) d^3\mathbf{x} d^3\mathbf{v} = 1. \tag{4.5}$$

The Boltzmann Equation is commonly written as:

$$\mathbf{L}[f] = \mathbf{C}[f], \tag{4.6}$$

where $\mathbf{L}$ and $\mathbf{C}$ are the Liouville and collision operators, respectively. The Liouville operator, taking into consideration that $\mathbf{v}$ is associated with momentum $\mathbf{p}$ in classical mechanics, can be expressed as:

$$\begin{aligned}\mathbf{L}[f] &= \frac{\mathrm{d}f}{\mathrm{d}t} \\ &= \frac{\partial f}{\partial t} + \sum_i \left(\frac{\partial f}{\partial q_i}\frac{\mathrm{d}q_i}{\mathrm{d}t} + \frac{\partial f}{\partial p_i}\frac{\partial p_i}{\partial t} \right) \\ &= \frac{\partial f}{\partial t} + \{f, H\},\end{aligned} \tag{4.7}$$

where $\{f, H\}$ is the Poisson bracket and H the Hamiltonian function. In the most general form, using relativistic notation, Equation (4.7) can be written as:

$$\begin{aligned}\mathbf{L}[f] &= \frac{\mathrm{d}f}{\mathrm{d}t} \\ &= \frac{\partial f}{\partial x^\mu}\frac{\mathrm{d}x^\mu}{\mathrm{d}t} + \frac{\partial f}{\partial p^\mu}\frac{\mathrm{d}p^\mu}{\mathrm{d}t} \\ &= \frac{\partial f}{\partial x^\mu}p^\mu + \frac{\partial f}{\partial p^\mu}\frac{\mathrm{d}p^\mu}{\mathrm{d}t}.\end{aligned} \tag{4.8}$$

From the General Relativity formalism it is known that the geodesic equation [6] is :

$$\begin{aligned}\frac{\mathrm{d}p^\mu}{\mathrm{d}t} + \Gamma^\mu_{\nu\lambda}p^\nu p^\lambda &= 0 \\ \frac{\mathrm{d}p^\mu}{\mathrm{d}t} &= -\Gamma^\mu_{\nu\lambda}p^\nu p^\lambda,\end{aligned} \tag{4.9}$$

where $\Gamma^\mu_{\nu\lambda}$ are the Christoffel symbols, related to the geometry of the space-time, x^μ is the $4-$position vector and p^μ is the $4-$momentum vector. Considering this, the Liouville operator is:

$$\mathbf{L}[f] = p^\mu\frac{\partial f}{\partial x^\mu} - \Gamma^\mu_{\nu\lambda}p^\nu p^\lambda\frac{\partial f}{\partial p^\mu}. \tag{4.10}$$

We can find a solution to Equation (4.7) using the Jeans theorem [7]. This theorem says that a solution to the Boltzmann equation must depend on an

integral of motion, that is to say, a function that depends on the positions and velocities, but no explicitly on time.

If ε is an integral of motion, for the case of one dimension, then:

$$\frac{\mathrm{d}\varepsilon}{\mathrm{d}t} = \frac{\partial\varepsilon}{\partial x}v + \frac{\partial\varepsilon}{\partial v}\dot{v} = 0, \tag{4.11}$$

In the case of a system with only gravitational interactions, ε could be obtained from Euler-Lagrange equation:

$$\frac{\partial\mathcal{L}}{\partial x} - \frac{\mathrm{d}}{\mathrm{d}t}\left(\frac{\partial\mathcal{L}}{\partial v}\right) = 0. \tag{4.12}$$

For the gravitational case $\mathcal{L} = \frac{1}{2}mv^2 + m\phi(x)$, where $\phi(x)$ is $\phi(x) = -\frac{U(x)}{m}$ and $U(x)$ is the gravitational potential energy. Then the Euler-Lagrange equation turns into:

$$\frac{\partial\phi}{\partial x} - \dot{v} = 0. \tag{4.13}$$

Multiplying by v at both sides of the equation before it is possible to obtain:

$$\frac{\partial\phi}{\partial x}v - v\dot{v} = 0. \tag{4.14}$$

Since $\frac{\partial\varepsilon}{\partial x}v + \frac{\partial\varepsilon}{\partial v}\dot{v} = 0$, then, comparing this equation with Equation (4.14) it is possible to say that that:

$$\frac{\partial\varepsilon}{\partial x} = \frac{\partial\phi}{\partial x}, \qquad \frac{\partial\varepsilon}{\partial v} = -v. \tag{4.15}$$

Solving this system of equations we find:

$$\varepsilon = \phi - \frac{1}{2}v^2. \tag{4.16}$$

In general, for more dimensions, ε is:

$$\varepsilon = \phi(r) - \frac{1}{2}|\mathbf{v}|^2 \tag{4.17}$$

where r is the radial variable in the spherical coordinate system. Since ε is the integral of motion associated with a system with only gravitational interactions. Then, using the Jeans theorem it is possible to say that $f(\mathbf{x}, \mathbf{v})$ must comply with $f(\mathbf{x}, \mathbf{v}) = f(\varepsilon)$.

Other solutions to the Boltzmann equation could include a dependency on total angular momentum (or angular momentum in z direction), leading to different velocity distributions.

In the case discussed above, where only kinetic energy and gravitational interactions rules, as happens in the Maxwell-Boltzmann distribution, an expression for $f(\varepsilon)$ can be proposed: $f(\varepsilon) \propto e^{\varepsilon/\sigma^2}$, where σ is the velocity dispersion. The probability density distribution associated with $f(\varepsilon)$ is shown in Equation (4.18):

$$\begin{aligned}\rho &\propto \int_0^\infty dv v^2 \exp\left\{\left(\frac{\phi - \frac{1}{2}v^2}{\sigma^2}\right)\right\} = \exp\left\{\frac{\phi}{\sigma^2}\right\}\int_0^\infty dv v^2 \exp\left\{-\left(\frac{v^2}{2\sigma^2}\right)\right\} \\ &\propto e^{\frac{\phi}{\sigma^2}}.\end{aligned} \tag{4.18}$$

In consequence, the gravitational potential $\phi(r)$ is:

$$\phi \propto \sigma^2 ln\rho. \tag{4.19}$$

In order to find an explicit expression for $\rho(r)$ only in terms of r it is necessary to use the gravitational Poisson equation, that relate gravitational the potential ϕ and density $\rho(r)$:

$$\begin{aligned} \nabla^2\phi(r) &= -4\pi G\rho(r) \\ \nabla^2 ln(\rho(r)) &= -\frac{4\pi G}{\sigma^2}\rho(r) \\ \frac{1}{r^2}\frac{\mathrm{d}}{\mathrm{d}r}\left(r^2\frac{\mathrm{d}ln(\rho)}{\mathrm{d}r}\right) &= -\frac{4\pi G}{\sigma^2}\rho(r). \end{aligned} \tag{4.20}$$

Assuming a solution of the form $\rho(r) = Cr^\alpha$, where C and α are constants, Equation (4.20) turns into:

$$\alpha r^{-2} = -\frac{4\pi G}{\sigma^2}Cr^\alpha, \tag{4.21}$$

and, in consequence $\alpha = -2$, $C = \dfrac{\sigma^2}{2\pi G}$, leading to the next result:

$$\rho(r) = \frac{\sigma^2}{2\pi G r^2}. \tag{4.22}$$

4.1.3 Density Distributions From Numerical Simulations

The resulting expression for the DM halo density, shown in Equation (4.22), is a good approximation, although collisions of particles have not been included. This is a reasonable approach given the fact that the Milky Way has not had a major merge with another galaxy in over 10 Gyears. Nevertheless, in order to improve the model minor merging processes have to be considered. This can be performed through numerical simulations of N-bodies. The simulations show that the density distribution for the DM halo, for a large number of galaxies, can be included as:

$$\rho_{NFW}(r) = \frac{\rho_0}{\frac{r}{r_s}\left(1+\frac{r}{r_s}\right)^2}, \tag{4.23}$$

where $r_s = 20\,Kpc$. Radial dependence is different from the model described by (4.20), showing that this model is incomplete. Another preferred

model for the density profile of DM is the Einasto model [4], with a density distribution shown in (4.24):

$$\rho_{Ein} = \rho_0 \left[-\frac{2}{\gamma} \left(\left(\frac{r}{r_s} \right)^{\gamma} - 1 \right) \right], \tag{4.24}$$

where $r_s = 20\, Kpc$ and $\gamma = 0,17$. In hydrodynamic simulations Burkert model becomes important . The density distribution associated with Burkert model is:

$$\rho_{Burk} = \frac{\rho_0}{\left(1 + \frac{r}{r_s}\right)\left(1 + \left(\frac{r}{r_s}\right)^2\right)}. \tag{4.25}$$

The Burkert model can describe the observational evidence from dwarf galaxies.

All of the previous density distributions differ from the model in Equation (4.22), showing that Maxwell-Boltzmann distribution does not yield the correct velocity distribution for DM.

Figure (4.1) shows the `Via Lactea` simulations [4] in comparison to a Maxwellian distribution fit of the data

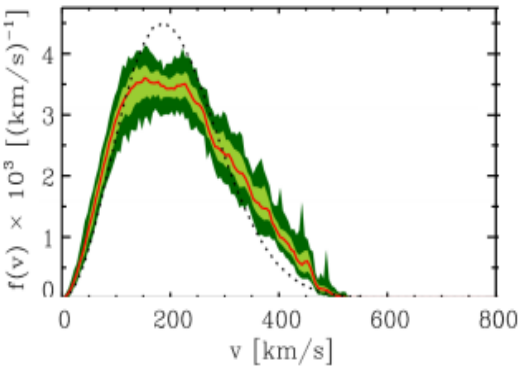

Figure 4.1: Velocity distribution for "Via Lactea" simulation. Figure taken from [4]

The distribution that is used most often in the literature is the Standard Halo Model (or truncated Maxwellian model), presented in Equation (4.26):

$$f(\mathbf{v}) = \begin{cases} \frac{1}{N_{esc}}\left(\frac{3}{2\pi\sigma_v^2}\right)^{3/2} e^{-3\mathbf{v}^2/2\sigma_v^2} & : |\mathbf{v}| < v_{esc} \\ \\ 0 & : \text{otherwise,} \end{cases} \tag{4.26}$$

where σ_v is the root mean square velocity dispersion, $v_0 = \sqrt{2/3}\sigma_v \approx 235\,km/s$ is the most probable speed, $N_{esc} = erf(z) - \frac{2}{\sqrt{\pi}} z e^{-z^2}$ with $z \equiv v_{esc}/v_0$, $erf(z) = \frac{2}{\sqrt{\pi}} \int_0^z e^{-x^2} \mathrm{d}x$ and v_{esc} the escape velocity. Equation (4.26) have the same structure of the Maxwell distribution [8], except for the factor $\frac{1}{N_{esc}}$ and its domain.

N-body simulations show that DM may form substructures, caused by tidal effects that strip DM in the case when another DM sub-halo falls into an orbit about the center of the galaxy, leaving remnants out of equilibrium which exhibits unique features that may affect observations. Examples of substructures include:

- **Clumps**: Merging can left clumps of DM, that would result in a localized over-density of DM.
- **Streams**: Debris left behind along the orbits of in-falling sub-halos, that make a tidal stream.
- **Debris Flow**: Sum total of the overlapping streams, shells, and plumes of debris from mergers. Debris flow accounts for the excess of particles on the tail of the `Via Lactea` distribution [4], relative to the Maxwellian expectation.
- **Dark Disk**: From N-body simulations we can find that a dark disk may form if sub-halos merging with the Milky Way are dragged through and disrupted by the baryonic disk [4].

4.1.4 Particle Physics Properties of Dark Matter

It is possible to make some general statements about the mass range of DM particles, only requiring that DM form halos. The expressions for the mass of the DM particle changes as a consequence of the spin-statistics of the particle [4].

If the particle is a Boson, then the exclusion principle shows that the occupation number is high and the problem is reduced to the next classical application of the uncertainty principle:

$$\begin{aligned} \Delta x \Delta p &\sim 1 \\ (2R_{halo})(m_\chi v) &\sim 1 \\ m_\chi &\sim \frac{1}{2R_{halo}v}, \end{aligned} \tag{4.27}$$

with v representing the velocity of the DM halo and m_χ the mass of the DM particle. From Dark Matter halos of dwarf galaxies [4], the mass m_χ for a scalar particle have the range:

$$m_\chi \geq 10^{-22}\, eV. \tag{4.28}$$

On the other hand, if the DM particle is a Fermion, as a consequence of the exclusion principle, the occupation number is low. In addition, taking in to account that the maximum of the Fermi-Dirac distribution [9] is $f(E,t) = 1$, the mass of the halo can be calculated as follows:

$$\begin{aligned} M_{halo} &= m_\chi V \int f(E,t) \mathrm{d}^3 p \\ &\leq m_\chi V \int \mathrm{d}^3 p \\ &\leq m_\chi^4 V v^3, \end{aligned} \tag{4.29}$$

with V representing the volume of the DM spherical halo and v its velocity. Using v as the virial velocity from Equation (4.4), then

$$\begin{aligned} M_{halo} &\leq m_\chi^4 G^{3/2} R_{halo}^{3/2} M_{halo}^{3/2} \\ m_\chi^4 &\geq (M_{halo} G^3 R_{halo}^3)^{-1/2} \\ m_\chi &\geq (M_{halo} G^3 R_{halo}^3)^{-1/8}. \end{aligned} \tag{4.30}$$

Phase-space densities of dwarf galaxies suggest that [4], in this case

$$m_\chi \geq 0.7\, KeV. \tag{4.31}$$

4.1.5 Thermal Dark Matter

Some time after the big-bang, both baryonic matter and DM formed. At this time the collisions among particles were abundant, so there must have been processes like $\chi\chi \to XX$, $XX \to \chi\chi$ and $\chi X \to \chi X$(with χ a DM particle and X a Standard Model particle). However, as the universe expanded it cooled down which consequently reduced the probability of collisions and the energy of the interactions, making DM creation and annihilation processes more and more unlikely to happen. The stage at which the universe has expanded and cooled down enough such that the rate of DM particles can be considered stable, is refereed to as the Freeze-out. The annihilation rate at Freeze-out is given by:

$$\Gamma_{inelastic} = n_\chi \langle \sigma v \rangle \tag{4.32}$$

where $\langle \sigma v \rangle$ is the velocity-averaged cross section and n_χ is the DM number density, that is defined by the following expression:

$$n = g \int f(E,t) \frac{\mathrm{d}^3 p}{(2\pi\hbar)^3}, \tag{4.33}$$

where g is the number of degrees of freedom of the DM particle. In the non-relativistic case the kinetic energy is $E = \frac{p^2}{2m_\chi}$ and the number density of DM particles is given by :

$$
\begin{aligned}
n_\chi &= g \int \frac{1}{\left(\exp\left\{\beta\left(\frac{p^2}{2m_\chi} - \mu\right)\right\} \pm 1\right)} \frac{\mathrm{d}^3 p}{(2\pi\hbar)^3} \\
&\sim T^{3/2} e^{-m_\chi/T},
\end{aligned}
\tag{4.34}
$$

where T is the temperature of a group of DM particles. In the ultra-relativistic case the kinetic energy is $E = \sqrt{p^2c^2 + m_\chi^2 c^4} \approx \sqrt{p^2c^2} \approx pc$ and in consequence:

$$
\begin{aligned}
n_\chi &= g \int \frac{1}{(\exp\{\beta(pc - \mu)\} \pm 1)} \frac{\mathrm{d}^3 p}{(2\pi\hbar)^3} \\
&\sim T^3.
\end{aligned}
\tag{4.35}
$$

4.2 The Energy Composition of the Universe: Basic Cosmological Principles in a Nutshell.

The cosmological model that should describe the universe must be one that considers its expansion and the cosmological principle: The universe is homogeneous and isotropic (as far as we know). The Friedmann-Lemaitre-Robertson-Walker (FLRW) model is the one that comply with these requirements. This model is represented by the metric (or space-time line element) in natural units:

$$
\begin{aligned}
ds^2 &= dt^2 - a^2(t)\left(\frac{dr^2}{1 - kr^2} + r^2 d\theta^2 + r^2 \sin^2\theta d\phi^2\right) \\
&= g_{\mu\nu} dx^\mu dx^\nu,
\end{aligned}
\tag{4.36}
$$

and the Einstein equations for the General Relativity:

$$
R_{\mu\nu} - \frac{1}{2} R g_{\mu\nu} + \Lambda g_{\mu\nu} = 8\pi G T_{\mu\nu},
\tag{4.37}
$$

where $a(t)$ is the scale distance factor (allows to associate an actual distance between two points of space with the same distance at a time t),dx_μ is the differentiated position four-vector (in spherical coordinates),ϕ, θ are the angular spherical variables, k the Gaussian curvature (intrinsic curvature in each point of a surface) for $a(t) = 1$ (today), $R_{\mu\nu}$ is the Ricci tensor, R is the Ricci scalar curvature ($R = g^{\mu\nu}R_{\mu\nu}$), $g_{\mu\nu}$ is the metric tensor, Λ is the cosmological constant and $T_{\mu\nu}$ is the energy-momentum tensor.

The way the scale factor associate an actual distance between two points of space with the same distance at a time t can be described through the following equation:

$$r = a(t)x, \tag{4.38}$$

where x is the actual distance between two points in the universe and r is the distance at a time t.

To complete the description of all the terms in Equation (4.37), it is necessary to show three equations: the first one for the explicit form of the metric tensor associated with Equation (4.36), the second one for the Ricci tensor, and the third one for the energy-momentum tensor. For the first equation, the metric tensor $g^{\mu\nu}$ can be derived directly from Equation (4.36) as:

$$g_{\mu\nu} = \begin{pmatrix} 1 & 0 & 0 & 0 \\ 0 & -\frac{a^2(t)}{1-kr^2} & 0 & 0 \\ 0 & 0 & -a^2(t)r^2 & 0 \\ 0 & 0 & 0 & -a^2(t)r^2\sin\theta \end{pmatrix}. \tag{4.39}$$

For the second equation, the Ricci tensor is defined as:

$$R_{\mu\nu} = \partial_\alpha \Gamma^\alpha_{\nu\mu} - \partial_\nu \Gamma^\alpha_{\alpha\mu} + \Gamma^\alpha_{\alpha\beta}\Gamma^\beta_{\nu\mu} - \Gamma^\alpha_{\nu\beta}\Gamma^\beta_{\alpha\mu} \tag{4.40}$$

where $\partial_\alpha = \dfrac{\partial}{\partial x^\alpha}$ and $\Gamma^\alpha_{\beta\gamma}$ are the Christoffel symbols, represented by:

$$\Gamma^\alpha_{\beta\gamma} = \frac{1}{2}g^{\alpha\mu}(\partial_\gamma g_{\mu\beta} + \partial_\beta g_{\mu\gamma} - \partial_\mu g_{\beta\gamma}). \tag{4.41}$$

Finally, for the third equation the general expression for energy-momentum tensor is:

$$T^{\mu\nu} = (\rho(t) + p(t))u^\mu u^\nu - p(t)g^{\mu\nu} \tag{4.42}$$

where u^μ is the velocity four-vector, $\rho(t)$ is the total energy density in the universe due to matter and radiation and $p(t)$ its corresponding pressure.

If the universe is considered homogeneous and isotropic, then it can be described as a perfect fluid. In fact, if the cosmological principle must be fulfilled, and the universe is considered as a fluid of matter and radiation, then the fluid must be a perfect fluid, i.e., a fluid without anisotropic stresses in a comoving frame (proper frame).

If a comoving frame is considered, then $u^\mu = (1, 0, 0, 0)$ and, using Equation (4.42), the explicit matrix form of $T^{\mu\nu}$ is

$$T^{\mu\nu} = \begin{pmatrix} \rho(t) & 0 & 0 & 0 \\ 0 & p(t)\frac{1-kr^2}{a^2(t)} & 0 & 0 \\ 0 & 0 & \frac{p(t)}{a^2(t)r^2} & 0 \\ 0 & 0 & 0 & \frac{p(t)}{a^2(t)r^2\sin^2\theta} \end{pmatrix}. \tag{4.43}$$

With all the considerations discussed above, it is possible to find the equations that describe the FLRW cosmological model. The 00 component of the Equation (4.37) is the Friedmann equation

$$\begin{aligned} \left(\frac{\dot{a}(t)}{a(t)}\right)^2 + \frac{k}{a^2} - \frac{\Lambda}{3} &= \frac{8\pi G\rho(t)}{3} \\ \left(\frac{\dot{a}(t)}{a(t)}\right)^2 + \frac{k}{a^2} &= \frac{8\pi G\left(\rho(t) + \frac{\Lambda}{8\pi G}\right)}{3} \end{aligned} \tag{4.44}$$

Taking in count that the total energy density $\rho(t)$ comes from the matter and radiation components of the universe, then $\rho(t) = \rho_m(t) + \rho_r(t)$ where $\rho_m(t)$ is the matter (and DM) energy density in the universe for any time

and ρ_r is the radiation energy density. Calling $\rho_\Lambda = \dfrac{\Lambda}{8\pi G}$, then the Equation (4.44) becomes

$$\begin{aligned}\left(\frac{\dot{a}(t)}{a(t)}\right)^2 + \frac{k}{a^2} &= 8\pi G\frac{\rho_m(t) + \rho_r(t) + \rho_\Lambda(t)}{3} \\ \left(\frac{\dot{a}(t)}{a(t)}\right)^2 + \frac{k}{a^2} &= 8\pi G\frac{\rho_t(t)}{3},\end{aligned} \tag{4.45}$$

where $\rho_t(t) = \rho_m(t) + \rho_r(t) + \rho_\Lambda(t)$.

The $11, 22$ and 33 components of the Equation (4.37) leads to the next equation

$$\begin{aligned}2\frac{\ddot{a}(t)}{a(t)} + \left(\frac{\dot{a}(t)}{a(t)}\right)^2 + \frac{k}{a^2(t)} - \Lambda &= -8\pi G p(t) \\ 2\frac{\ddot{a}(t)}{a(t)} + \left(\frac{\dot{a}(t)}{a(t)}\right)^2 + \frac{k}{a^2(t)} &= -8\pi G\left(p(t) - \frac{\Lambda}{8\pi G}\right)\end{aligned} \tag{4.46}$$

The pressure $p(t)$, as it was previously said is due to matter and radiation, then $p(t) = p_m(t) + p_r(t)$, where $p_m(t)$ is the matter(and DM) energy pressure and $p_r(t)$ is the radiation pressure. Calling $p_\Lambda = -\frac{\Lambda}{8\pi G}$, the Equation (4.46) can be written as

$$\begin{aligned}2\frac{\ddot{a}(t)}{a(t)} + \left(\frac{\dot{a}(t)}{a(t)}\right)^2 + \frac{k}{a^2(t)} &= -8\pi G(p_m(t) + p_r(t) + p_\Lambda(t)) \\ &= -8\pi G p_t(t)\end{aligned} \tag{4.47}$$

where $p_t(t) = p_m(t) + p_r(t) + p_\Lambda(t)$. In the literature, $\rho_\Lambda(t)$ and $p_\Lambda(t)$ are called vacuum energy density and vacuum pressure respectively.

The conservation of energy in the General Relativity is expressed in the next equation

$$D_\mu T^{\mu\nu} = \frac{\partial T^{\mu\nu}}{\partial x^\mu} + \Gamma^\mu_{\mu\sigma} T^{\sigma\nu} + \Gamma^\nu_{\mu\sigma} T^{\mu\sigma} = 0 \tag{4.48}$$

where $D_\mu T^{\mu\nu}$ is the covariant derivative of the tensor $T^{\mu\nu}$, that is, a generalization of the partial derivative in curvilinear spaces.

Taking $\nu = 0$ in Equation (4.48) then

$$\frac{\partial T^{\mu 0}}{\partial x^\mu} + \Gamma^\mu_{\mu\sigma} T^{\sigma 0} + \Gamma^0_{\mu\sigma} T^{\mu\sigma} = 0 \tag{4.49}$$

Since the energy-momentum tensor is diagonal, then $T^{\mu\nu} = 0$ if $\mu \neq \nu$ and the Equation (4.49) becomes

$$\frac{\partial T^{00}}{\partial x^0} + \Gamma^\mu_{\mu 0} T^{00} + \Gamma^0_{\mu\mu} T^{\mu\mu} = 0. \tag{4.50}$$

Taking in count all the non-zero Christoffel symbols in the Appendix, then the Equation (4.50) is now

$$\dot{\rho}(t) + 3\frac{\dot{a}(t)}{a(t)}(\rho(t) + p(t)) = 0. \tag{4.51}$$

The Equation (4.51) is in terms of both $\rho_m(t), p_m(t)$ and $\rho_r(t), p_r(t)$ implicitly, but is valid too for each independent component of the universe (including dark energy) [10], that is to say

$$\dot{\rho}_i(t) + 3\frac{\dot{a}(t)}{a(t)}(\rho_i(t) + p_i(t)) = 0 \tag{4.52}$$

where $i = m, r, \Lambda$. The Equations (4.45), (4.47) and (4.52) describe the FLRW cosmological model.

From thermodynamics it is possible to relate $\rho_i(t)$ and $p_i(t)$ [10] through the relation

$$p_i(t) = \omega_i \rho_i(t) \tag{4.53}$$

where

$$\omega_i = \begin{cases} 0 & i = m \\ \frac{1}{3} & i = r \\ -1 & i = \Lambda \end{cases} \tag{4.54}$$

Using the Equations (4.52) and (4.54) it is possible to find that

$$\begin{aligned} &\dot{\rho}_i(t) + 3\frac{\dot{a}(t)}{a(t)}(1+\omega_i)\rho_i(t) = 0 \\ &\frac{\dot{\rho}(t)}{\rho(t)} = -3(1+\omega_i)\frac{\dot{a}(t)}{a(t)} \\ &d[ln(\rho_i(t))] = d[-3(1+\omega_i)ln(a(t))] \\ &ln(\rho_i(t)) = -3(1+\omega_i)ln(a(t)) + C_1 \\ &ln(\rho_i(t)) = ln(C_2(a(t))^{-3(1+\omega_i)}) \\ &\rho_i(t) = C_2(a(t))^{-3(1+\omega_i)} \end{aligned} \tag{4.55}$$

where C_1 is a constant and $C_2 = e^{C_1}$.

For the case of radiation $\omega_i = \frac{1}{3}$, in consequence the Equation (4.55) becomes

$$\rho_r(t) = C_2 a^{-4}(t). \tag{4.56}$$

From Equation (4.38) is possible to deduce that, in the actual time t_0, the scale factor is $a(t_0) = 1$, because in t_0 the distance r needs to be equal to the actual distance x. Taking in count the argument above, then from Equation (4.56) it is possible to deduce that

$$\rho_r(t_0) = C_2, \tag{4.57}$$

and Equation (4.56) is now

$$\rho_r(t) = \rho_r(t_0) a^{-4}(t). \tag{4.58}$$

From the Stefan-Boltzmann law it is possible to relate $\rho_r(t)$ and temperature. The relation between radiation energy density and temperature is

$$\rho_r(t) = CT^4(t), \tag{4.59}$$

where C is a constant. In the actual time Equation (4.59) becomes

$$\rho_r(t_0) = CT_0^4 \tag{4.60}$$

with T_0 the actual temperature of the Cosmic Microwave Background. Using Equations (4.58), (4.59) and (4.60) it is possible to observe that

$$\begin{aligned} CT^4(t) &= CT_0^4 a^{-4}(t) \\ T(t) &= \frac{T_0}{a(t)} \end{aligned} \tag{4.61}$$

4.3 An Introduction to Dark Matter

4.3.1 Collisionless Boltzmann Equation

The number density of any type of particle in the universe is defined as

$$n = \frac{N}{V}, \tag{4.62}$$

where N is the number of particles and V is the volume of the universe. If the cosmological principle is used, that is, a homogeneous and isotropic universe, a spherically symmetric model of the universe can be taken. In consequence V can be written as $V = \frac{4}{3}\pi r^3$, where r is the "radius" of the universe. If the FLRW cosmological model [11] is considered, r is defined by the Equation (4.38).

With Equation (4.38) and the considerations above, Equation (4.62) can be written as

$$n = \frac{N}{\frac{4}{3}\pi a^3(t)x^3} = \frac{3N}{4\pi a^3(t)x^3}. \tag{4.63}$$

The change in time of number density is

$$\begin{aligned} \frac{\mathrm{d}n}{\mathrm{d}t} &= \frac{3N}{4\pi x^3}\frac{\mathrm{d}}{\mathrm{d}t}\left(\frac{1}{a^3(t)}\right) \\ &= \frac{3N}{4\pi x^3}\left(-\frac{3\dot{a}(t)}{a^4(t)}\right) \\ &= -3\frac{\dot{a}(t)}{a(t)}n. \end{aligned} \tag{4.64}$$

Equation (4.64) can be reexpressed as

$$\begin{aligned} \frac{\mathrm{d}n}{\mathrm{d}t} + 3\frac{\dot{a}(t)}{a(t)}n &= 0 \\ \frac{1}{a^3(t)}\frac{\mathrm{d}}{\mathrm{d}t}\big(na^3(t)\big) &= 0 \end{aligned} \tag{4.65}$$

The Equation (4.65) is the Boltzmann equation for a collisionless system, i.e the collision operator $\mathbf{C}[f] = 0$. Equation (4.63) allow to write the Equation (4.65) as

$$\begin{aligned} \frac{1}{a^3(t)}\frac{\mathrm{d}}{\mathrm{d}t}\left(\frac{3N}{4\pi x^3}\right) &= 0 \\ \frac{\mathrm{d}N}{\mathrm{d}t} &= 0. \end{aligned} \tag{4.66}$$

The Equation (4.66) indicates that the number of particles N remains constant in time, as a consequence of taking $\mathbf{C}[f] = 0$, only considering the expansion of the universe.

4.3.2 Boltzmann Equation with Collision Terms

In order to include the collisional term in Equation (4.65), is necessary to understand the interaction between particles in collision processes. If the process $1 + 2 \leftrightarrow 3 + 4$ is considered, then the Boltzmann equation with the collision term can be written as

$$\frac{1}{a^3(t)}\frac{\mathrm{d}}{\mathrm{d}t}\big(n_i a^3(t)\big) = -\alpha n_1 n_2 + \beta n_3 n_4 \tag{4.67}$$

because the annihilation part of the process depends on the nature of the particles 1 and 2 and the creation part depends on the nature of particles 3 and 4 (specifically in their number densities). In Equation (4.67) n_1, n_2, n_3 and n_4 are the number densities of particles $1, 2, 3$ and 4, respectively, $i = 1, 2, 3, 4$, α represents the velocity-averaged annihilation cross section for n_1 and n_2, represented as $\langle \sigma v \rangle_{1,2}$, where v is the Moller velocity and the minus sign next to α represent the fact that in the annihilation process n_1 and n_2 decreases.

When the system is in equilibrium, i.e the system properties does not change in time, then Equation (4.67) becomes

$$0 = -\alpha n_1^{eq} n_2^{eq} + \beta n_3^{eq} n_4^{eq} \tag{4.68}$$

and, in consequense

$$\beta = \alpha \frac{n_1^{eq} n_2^{eq}}{n_3^{eq} n_4^{eq}} \tag{4.69}$$

and Equation (4.67) can be written as

$$\frac{1}{a^3(t)}\frac{\mathrm{d}}{\mathrm{d}t}\big(n_i a^3(t)\big) = -\alpha\left(n_1 n_2 - \frac{n_1^{eq} n_2^{eq}}{n_3^{eq} n_4^{eq}} n_3 n_4\right) \tag{4.70}$$

Now, if the case of the collision of two DM particles is considered, then particles 1 and 2 are DM particles (χ) while particles 3 and 4 are particles of Standard Model. With the consideration before it is possible to say that $n_1 = n_2 = n$ and Equation (4.70) takes the form

$$\frac{1}{a^3(t)}\frac{\mathrm{d}}{\mathrm{d}t}\big(n_i a^3(t)\big) = -\alpha\left(n^2 - \frac{n_{eq}^2}{n_3^{eq}n_4^{eq}}n_3 n_4\right). \tag{4.71}$$

Assuming that particles 3 and 4, as soon as they are produced, go to kinetic and chemical equilibrium with other particles and the temperature T_i of any specie composed of the particles 3 or 4 comply with $T_i << E_i - \mu_i$, where E_i is the total energy of each species and μ_i its chemical potential, then $n_3 n_4 = n_3^{eq} n_4^{eq}$,because with all the considerations before the density phase-space distribution f goes from Fermi-Dirac or Bose-Einstein distributions to Maxwell-Boltzmann distribution, that only depends on E_i.

The Equation (4.71), with all the considerations above becomes

$$\begin{aligned}\frac{1}{a^3(t)}\frac{\mathrm{d}}{\mathrm{d}t}\big(n_i a^3(t)\big) &= -\alpha\big(n^2 - n_{eq}^2\big) \\ &= -\left\langle\sigma v\right\rangle_{1,2}\left(n^2 - n_{eq}^2\right)\end{aligned} \tag{4.72}$$

From the FLRW cosmological model [11] is known that the temperature of the universe $T(t)$ is related to the scale factor $a(t)$ by the Equation (4.61). Taking Equation (4.61) in count, then the Boltzmann equation (4.72) becomes

$$T^3(t)\frac{\mathrm{d}}{\mathrm{d}t}\left(\frac{n_i}{T^3(t)}\right) = -\left\langle\sigma v\right\rangle_{1,2}\left(n^2 - n_{eq}^2\right) \tag{4.73}$$

Defining $Y = \dfrac{n_i}{T^3(t)}$, then Equation (4.73) takes the form

$$\frac{\mathrm{d}Y}{\mathrm{d}t} = -T^3(t)\left\langle\sigma v\right\rangle_{1,2}\left(Y^2 - Y_{eq}^2\right) \tag{4.74}$$

Defining yet another variable $x = \dfrac{m_\chi c^2}{k_B T(t)} = \dfrac{m_\chi c^2 a(t)}{k_B T_0}$ to describe a variable related with time in term of temperature (with c the speed of light in the vacuum and k_B the Boltzmann constant), and using the fact that

$\frac{\mathrm{d}Y}{\mathrm{d}t} = \frac{\mathrm{d}Y}{\mathrm{d}x}\frac{\mathrm{d}x}{\mathrm{d}t} = -x\frac{\dot{T}(t)}{T}\frac{\mathrm{d}Y}{\mathrm{d}x}$ thanks to the chain rule, then Equation (4.74) can be written as

$$\frac{\mathrm{d}Y}{\mathrm{d}x} = \frac{T(t)}{x\dot{T}(t)}T^3(t)\left\langle\sigma v\right\rangle_{1,2}(Y^2 - Y_{eq}^2) \tag{4.75}$$

The Hubble parameter $H(t)$ is defined as $H(t) = \frac{\dot{a}(t)}{a(t)}$, but in terms of temperature, $H(t)$ becomes

$$\begin{aligned} H(t) &= T(t)\frac{\mathrm{d}}{\mathrm{d}t}\left(\frac{1}{T(t)}\right) \\ &= -\frac{\dot{T}(t)}{T(t)}, \end{aligned} \tag{4.76}$$

and, in consequence Equation (4.75) becomes

$$\begin{aligned} \frac{\mathrm{d}Y}{\mathrm{d}x} &= -\frac{1}{xH(t)}T^3(t)\left\langle\sigma v\right\rangle_{1,2}(Y^2 - Y_{eq}^2) \\ &= -\frac{m_\chi^3 c^6}{k_B^3 x^4 H(t)}\left\langle\sigma v\right\rangle_{1,2}(Y^2 - Y_{eq}^2) \end{aligned} \tag{4.77}$$

A expression for Y_{eq} could be obtained from Statistical Physics. Assuming that, in equilibrium the chemical potential μ comply with $\mu << T$ (because there is no significant contribution of energy due to the change of density number), the density number, both for fermions and bosons is

$$\begin{aligned} n_{eq} &= g\int\frac{d^3p}{(2\pi\hbar)^3}\frac{1}{e^{E/k_BT}\pm 1} \\ &= \frac{4\pi}{(2\pi\hbar)^3}g\int_0^\infty dp\frac{p^2}{e^{E(p)/k_BT}\pm 1}, \qquad (E = E(p)) \end{aligned} \tag{4.78}$$

where g is the number of degrees of freedom of the particle and E the energy of the particle. If the general relativistic case is considered then $E^2 = p^2c^2 + m^2c^4$ and Equation (4.78) can be written as

$$n_{eq} = \frac{4\pi}{(2\pi\hbar)^3} g \int_0^\infty dp \frac{p^2}{\exp\left\{\frac{\sqrt{p^2c^2+m^2c^4}}{k_B T}\right\} \pm 1}. \tag{4.79}$$

If a classical approach is taking in count, then a series approximation of $E(p)$ is necessary. To second orden in p, the expression for $E(p)$ is

$$E(p) \approx mc^2 + \frac{p^2}{2m}, \tag{4.80}$$

and Equation (4.79) turns to be

$$n_{eq} = \frac{4\pi}{(2\pi\hbar)^3} g \int_0^\infty dp \frac{p^2}{\exp\left\{\frac{mc^2+\frac{p^2}{2m}}{k_B T}\right\} \pm 1}. \tag{4.81}$$

In the classical approximation there is another consideration: it must be fulfilled that $mc^2 >> k_B T$. With the consideration before, the exponential term $\exp\left\{\frac{mc^2}{k_B T}\right\} >> 1$ and then the Equation (4.81) is now

$$
\begin{aligned}
n_{eq} &\approx \frac{4\pi}{(2\pi\hbar)^3} g \int_0^\infty dp \frac{p^2}{\exp\left\{\frac{mc^2+\frac{p^2}{2m}}{k_B T}\right\}} \\
&\approx \frac{g}{2\pi^2\hbar^3} \exp\left\{-\frac{mc^2}{k_B T}\right\} \int_0^\infty dp \exp\left\{-\frac{p^2}{2mk_B T}\right\} p^2 \\
&\approx \frac{g}{2\pi^2\hbar^3} \exp\left\{-\frac{mc^2}{k_B T}\right\} (2mk_B T)^{3/2} \int_0^\infty du \exp\{-u^2\} u^2 \qquad \left(u = \frac{p}{\sqrt{2mk_B T}}\right) \\
&\approx \frac{g}{2\pi^2\hbar^3} \exp\left\{-\frac{mc^2}{k_B T}\right\} (2mk_B T)^{3/2} \left(-\frac{\partial}{\partial\alpha} \int_0^\infty du \exp\{-\alpha u^2\}\right|_{\alpha=1} \\
&\approx \frac{g}{2\pi^2\hbar^3} \exp\left\{-\frac{mc^2}{k_B T}\right\} (2mk_B T)^{3/2} \left(-\frac{\partial}{\partial\alpha} \frac{1}{2}\sqrt{\frac{\pi}{\alpha}}\right|_{\alpha=1} \\
&\approx \frac{g}{2\pi^2\hbar^3} \exp\left\{-\frac{mc^2}{k_B T}\right\} (2mk_B T)^{3/2} \left(\frac{1}{4}\sqrt{\frac{\pi}{\alpha^3}}\right|_{\alpha=1} \\
&\approx g\left(\frac{mk_B T}{2\pi\hbar^2}\right)^{3/2} \exp\left\{-\frac{mc^2}{k_B T}\right\},
\end{aligned}
\tag{4.82}
$$

and, in consequense, Y_{eq} for a DM non -relativistic particle is

$$
\begin{aligned}
Y_{eq} &= \frac{n_{eq}}{T^3} \\
&\approx \frac{1}{T^3} g\left(\frac{m_\chi k_B T}{2\pi\hbar^2}\right)^{3/2} \exp\left\{-\frac{m_\chi c^2}{k_B T}\right\} \\
&\approx g\left(\frac{m_\chi k_B}{2\pi\hbar^2 T}\right)^{3/2} \exp\left\{-\frac{m_\chi c^2}{k_B T}\right\} \\
&\approx g\left(\frac{x k_B^2}{2\pi c^2\hbar^2}\right)^{3/2} e^{-x} \\
&= \frac{g}{(2\pi)^{3/2}} \left(\frac{k_B}{c\hbar}\right)^3 x^{3/2} e^{-x}.
\end{aligned}
\tag{4.83}
$$

For a relativistic particle, the momentum is greater than the product of mass of the particle and the velocity of light and this implies that $E(p) \approx pc$

(as it was discussed to derive Equation (4.35)) . With this consideration Equation (4.79) becomes

$$n_{eq} = \frac{g}{2\pi^2\hbar^3}\int_0^\infty dp \frac{p^2}{\exp\left\{\frac{pc}{k_BT}\right\} \pm 1}. \tag{4.84}$$

For bosons (the minus sign is chosen in the term $\exp\left\{\frac{pc}{k_BT}\right\} \pm 1$), n_{eq} is

$$\begin{aligned} n_{eq} &= \frac{g}{2\pi^2\hbar^3}\int_0^\infty dp \frac{p^2}{\exp\left\{\frac{pc}{k_BT}\right\} - 1} \\ &= \frac{g}{2\pi^2\hbar^3} 2\zeta(3)\frac{k_B^3T^3}{c^3} \\ &= g\frac{\zeta(3)}{\pi^2\hbar^3}\frac{k_B^3T^3}{c^3}, \end{aligned} \tag{4.85}$$

where $\zeta(s)$ is the Riemann zeta function and, for fermions (the plus sign is chosen in the term $\exp\left\{\frac{pc}{k_BT}\right\} \pm 1$), n_{eq} is

$$\begin{aligned} n_{eq} &= \frac{g}{2\pi^2\hbar^3}\int_0^\infty dp \frac{p^2}{\exp\left\{\frac{pc}{k_BT}\right\} + 1} \\ &= \frac{g}{2\pi^2\hbar^3}\frac{3}{2}\zeta(3)\frac{k_B^3T^3}{c^3} \\ &= \frac{3}{4}g\frac{\zeta(3)}{\pi^2\hbar^3}\frac{k_B^3T^3}{c^3}, \end{aligned} \tag{4.86}$$

The results in Equations (4.85) and (4.86) can be unify in one expression, that is

$$n_{eq}(T) = g_*\frac{\zeta(3)}{\pi^2\hbar^3}\frac{k_B^3T^3}{c^3}, \tag{4.87}$$

where g_* is $g_* = g$ for bosons and $g_* = \frac{3}{4}g$. Equation (4.87) considers that bosons and fermions are in equilibrium, but that is not the general case.

To include states with different temperatures, the term g_* must be modified, becoming a weighted sum over different temperatures of bosons and fermions [10]. The expression for g_* is

$$g_*(T) = \sum_{bosons} g_{bosons}\left(\frac{T_{bosons}}{T}\right)^3 + \sum_{fermions} \frac{3}{4} g_{fermions}\left(\frac{T_{fermions}}{T}\right)^3 \quad (4.88)$$

where g_{bosons},$g_{fermions}$ are the number of degrees of freedom of each Boson and Fermion considered and T_{bosons}, $T_{fermions}$ its temperatures. As a consequence of the things said before, the general expression for the number density is

$$n(T) = g_*(T)\frac{\zeta(3)}{\pi^2\hbar^3}\frac{k_B^3 T^3}{c^3}, \quad (4.89)$$

4.3.3 Boltzmann Equation in Different Points of the Thermal History of the Universe

In the FLRW cosmological model [11] is possible to identify three parts of the thermal history of the universe: Radiation era, Matter era and Dark energy era. Each of these parts have a specific expression for the scale factor and, in consequence, a different expression for the Hubble parameter. The Boltzmann equation will be analyzed below for each of the cases before.

Radiation era

The Friedmann Equation (4.45) for a plane universe ($k = 0$) is

$$H(t)^2 = \hbar c \frac{\rho_m(t) + \rho_r(t) + \rho_\Lambda(t)}{3M_{Pl}^2}. \quad (4.90)$$

where $M_{Pl} = \sqrt{\frac{\hbar c}{8\pi G}}$ is the reduced Planck mass.

A expression for ρ_r can be obtained from Statistical Physics too. In equilibrium, the expression for ρ_r is

$$\begin{aligned}\rho_{eq_r} &= g\int \frac{d^3p}{(2\pi\hbar)^3}\frac{E}{e^{E/T}\pm 1}\\ &= \frac{4\pi}{(2\pi\hbar)^3}g\int_0^\infty p^2dp\frac{E(p)}{e^{E(p)/k_BT}\pm 1}\\ &= \frac{4\pi}{(2\pi\hbar)^3}g\int_0^\infty p^2dp\frac{\sqrt{p^2c^2+m^2c^4}}{\exp\left\{\frac{\sqrt{p^2c^2+m^2c^4}}{k_BT}\right\}\pm 1}.\end{aligned} \tag{4.91}$$

In the relativistic limit $pc >> mc^2$, in consequense $E(p)\approx pc$ and Equation (4.91) turns to be

$$\begin{aligned}\rho_{eq_r} &= \frac{g}{2\pi^2\hbar^3}\int_0^\infty p^2dp\frac{pc}{\exp\left\{\frac{pc}{k_BT}\right\}\pm 1}\\ &= \frac{gc}{2\pi^2\hbar^3}\int_0^\infty dp\frac{p^3}{\exp\left\{\frac{pc}{k_BT}\right\}\pm 1}.\end{aligned} \tag{4.92}$$

For bosons (the minus sign is chosen in the term $\exp\left\{\frac{pc}{k_BT}\right\}\pm 1$), ρ_{eq_r} is

$$\begin{aligned}\rho_{eq_r} &= \frac{gc}{2\pi^2\hbar^3}\frac{\pi^4k_B^4T^4}{15c^4}\\ &= g\frac{\pi^2}{30}\frac{k_B^4}{c^3\hbar^3}T^4,\end{aligned} \tag{4.93}$$

and, for fermions (the plus sign is chosen in the term $\exp\left\{\frac{pc}{k_BT}\right\}\pm 1$), ρ_{eq_r} is

$$\begin{aligned}\rho_{eq_r} &= \frac{gc}{2\pi^2\hbar^3}\frac{7\pi^4k_B^4T^4}{120c^4}\\ &= \frac{7}{8}g\frac{\pi^2}{30}\frac{k_B^4}{c^3\hbar^3}gT^4.\end{aligned} \tag{4.94}$$

The results before can be expressed in the next equation

$$\rho_{eq_r} = g_{eff}\frac{\pi^2}{30}\frac{k_B^4}{c^3\hbar^3}T^4 \tag{4.95}$$

where $g_{eff} = g$ for bosons and $g_{eff} = \frac{7}{8}g$ for fermions.

Equation (4.95) considers that Bosons and Fermions are in equilibrium, but that is not the general case. To include states with different temperatures, the term g_{eff} must be modified, becoming a weighted sum over different temperatures of bosons and fermions [10]. The expression for g_{eff} is

$$g_{eff}(T) = \sum_{bosons} g_{bosons}\left(\frac{T_{bosons}}{T}\right)^4 + \sum_{fermions}\frac{7}{8}g_{fermions}\left(\frac{T_{fermions}}{T}\right)^4. \tag{4.96}$$

With all the considerations before, then the general expression for ρ_r in the relativistic case is

$$\rho_r = g_{eff}(T)\frac{\pi^2}{30}\frac{k_B^4}{c^3\hbar^3}T^4. \tag{4.97}$$

In the Radiation era, $\rho_r >> \rho_m$ and $\rho_r >> \rho_\Lambda$, and, in consequense, Equation (4.90) turns to be, in natural units

$$H(t)^2 \approx \frac{\rho_r}{3M_{Pl}^2}. \tag{4.98}$$

Taking in count the Equation (4.97) then

$$\begin{aligned} H(t) &\approx \frac{1}{M_{Pl}}\sqrt{\frac{\rho_r}{3}} \\ &\approx \frac{\pi T^2}{M_{Pl}}\sqrt{\frac{g_{eff}}{90}}, \end{aligned} \tag{4.99}$$

or, in terms of the variable x

$$H(x) \approx \frac{\pi m_\chi^2}{M_{Pl}}\sqrt{\frac{g_{eff}}{90}}\frac{1}{x^2}. \tag{4.100}$$

The Equation (4.77), for the Radiation era, taking in count the Equation (4.100) is

$$\frac{\mathrm{d}Y}{\mathrm{d}x} = -\frac{m_\chi M_{Pl}}{\pi x^2}\sqrt{\frac{90}{g_{eff}}}\,\langle\sigma v\rangle_{1,2}\,(Y^2 - Y_{eq}^2). \tag{4.101}$$

An illustration of the numerical solution of Equation (4.101) is shown in Figure 4.3

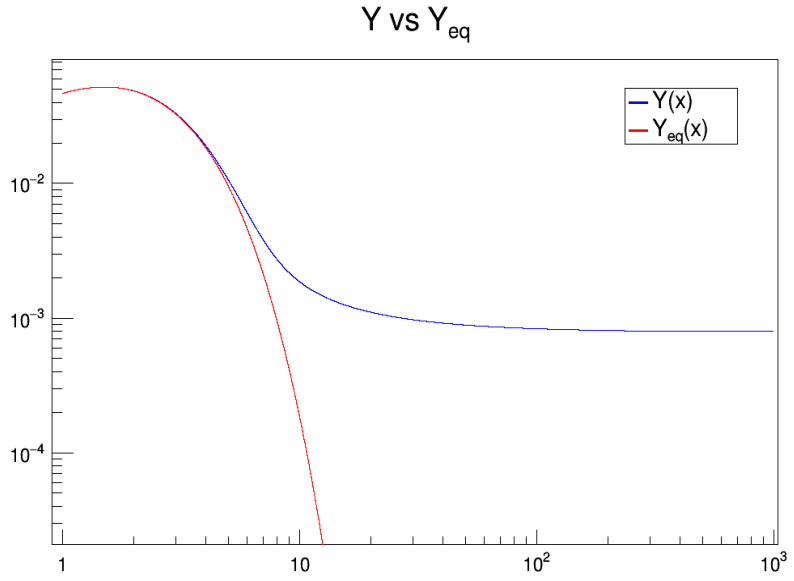

Figure 4.2: Illustration for Y vs x and Y_{eq} vs x obtained from a performing of Runge-Kutta Method of fouth order over Equation (4.101).

The Figure 4.3 shows that there is a point where Y and Y_{eq} differ and Y begins to be constant, this point is the Freeze-Out. In order to obtain the DM relic density, some approximations will be made from the results in Figure 4.3.

In the interval $x_f \leq x < \infty$ is clear that $Y >> Y_{eq}$ and, in consequence, in this interval

$$\begin{aligned}
\frac{\mathrm{d}Y}{\mathrm{d}x} &\approx -\frac{m_\chi M_{Pl}}{\pi}\sqrt{\frac{90}{g_{eff}}}\left\langle\sigma v\right\rangle_{1,2}\frac{Y^2}{x^2} \\
\int_{x_f}^{\infty}\frac{dY}{Y^2} &\approx -\frac{m_\chi M_{Pl}}{\pi}\sqrt{\frac{90}{g_{eff}}}\left\langle\sigma v\right\rangle_{1,2}\int_{x_f}^{\infty}\frac{dx}{x^2} \\
\frac{1}{Y_{x_f}} - \frac{1}{Y_\infty} &\approx -\frac{m_\chi M_{Pl}}{\pi}\sqrt{\frac{90}{g_{eff}}}\left\langle\sigma v\right\rangle_{1,2}\frac{1}{x_f}.
\end{aligned} \tag{4.102}$$

From Figure 4.3 is clear that $Y_{x_f} >> Y_\infty$ ($Y_\infty = Y_{today}$) and this leads to say that $\frac{1}{Y_{x_f}} << \frac{1}{Y_\infty}$. With all the considerations before then Equation (4.102) can be written as

$$\begin{aligned}
\frac{1}{Y_\infty} &\approx \frac{m_\chi M_{Pl}}{\pi}\sqrt{\frac{90}{g_{eff}}}\left\langle\sigma v\right\rangle_{1,2}\frac{1}{x_f} \\
Y_\infty &\approx \frac{\pi}{m_\chi M_{Pl}\left\langle\sigma v\right\rangle_{1,2}}\sqrt{\frac{g_{eff}}{90}}x_f.
\end{aligned} \tag{4.103}$$

The definition of mass density is

$$\rho = \frac{M}{V} \tag{4.104}$$

where M is the mass of certain specie and V its volume. For the case of Dark Matter, the mass density is

$$\begin{aligned}
\rho_\chi &= \frac{M_\chi}{V} \\
&= \frac{N m_\chi}{V} \\
&= n(T) m_\chi
\end{aligned} \tag{4.105}$$

Taking in count the Equation (4.105), the mass density of DM today ρ_{χ_0} is

$$\begin{aligned}
\rho_{\chi_0} &= n(T_0)m_\chi \\
&= n(T_\infty)\frac{n(T_0)}{n(T_\infty)}m_\chi \\
&= n(T_\infty)\left(\frac{a(T_\infty)}{a(T_0)}\right)^3 m_\chi \\
&= \frac{n(T_\infty)}{T_\infty^3}\left(\frac{a(T_\infty)T_\infty}{a(T_0)T_0}\right)^3 T_0^3 m_\chi \\
&= Y_\infty T_0^3 m_\chi
\end{aligned} \tag{4.106}$$

where the term $\left(\frac{a(T_\infty)T_\infty}{a(T_0)T_0}\right)^3 = 1$ because $a(t)T(t) = constant$ as shown in Equation (4.61). The density parameter Ω_{χ_0} associated with ρ_{χ_0} is, by definition

$$\Omega_{\chi_0} = \frac{\rho_{\chi_0}}{\rho_{c_0}} \tag{4.107}$$

where $\rho_{c_0} = 3M_{Pl}^2 H_0^2$ (in natural units) is the critical density, which is the mass density needed to have $k = 0$ and H_0 is the Hubble constant. The parameter Ω_{χ_0} is

$$\begin{aligned}
\Omega_{\chi_0} &= \frac{Y_\infty T_0^3 m_\chi}{3M_{Pl}^2 H_0^2} \\
&= \frac{\frac{\pi}{m_\chi M_{Pl}\langle\sigma v\rangle_{1,2}}\sqrt{\frac{g_{eff}}{90}}x_f T_0^3 m_\chi}{3M_{Pl}^2 H_0^2} \\
&= \frac{\pi}{3M_{Pl}^3 H_0^2 \langle\sigma v\rangle_{1,2}}\sqrt{\frac{g_{eff}}{90}}x_f T_0^3.
\end{aligned} \tag{4.108}$$

Now, considering that $a(t)T(t)$ is no longer a constant, then ρ_{χ_0} becomes

$$\begin{aligned}
\rho_{\chi_0} &= n(T_0)m_\chi \\
&= n(T_\infty)\frac{n(T_0)}{n(T_\infty)}m_\chi \\
&= n(T_\infty)\left(\frac{a(T_\infty)}{a(T_0)}\right)^3 m_\chi \\
&= n(T_\infty)\left(\frac{a(T_\infty)T_\infty}{a(T_0)T_0}\right)^3 \frac{T_0^3}{T_\infty^3}m_\chi \\
&= \frac{n(T_\infty)}{T_\infty^3}\left(\frac{a(T_\infty)T_\infty}{a(T_0)T_0}\right)^3 T_0^3 m_\chi \\
&= Y_\infty T_0^3 m_\chi \left(\frac{a(T_\infty)T_\infty}{a(T_0)T_0}\right)^3,
\end{aligned} \tag{4.109}$$

and, in consequence

$$\Omega_{\chi_0} = \frac{\pi}{3M_{Pl}^3 H_0^2 \langle\sigma v\rangle_{1,2}}\left(\frac{a(T_\infty)T_\infty}{a(T_0)T_0}\right)^3 \sqrt{\frac{g_{eff}}{90}}x_f T_0^3. \tag{4.110}$$

From Equation (4.89) it is possible to derive that

$$\begin{aligned}
\frac{n(T_0)}{n(T_\infty)} &= \frac{g_*(T_0)\frac{\zeta(3)}{\pi^2}\frac{k_B^3 T_0^3}{c^3}}{g_*(T_\infty)\frac{\zeta(3)}{\pi^2}\frac{k_B^3 T_\infty^3}{c^3}} \\
\left(\frac{a(T_\infty)}{a(T_0)}\right)^3 &= \frac{g_*(T_0)T_0^3}{g_*(T_\infty)T_\infty^3} \\
\left(\frac{a(T_\infty)T_\infty}{a(T_0)T_0}\right)^3 &= \frac{g_*(T_0)}{g_*(T_\infty)}.
\end{aligned} \tag{4.111}$$

The result obtained in Equation (4.111) shows that is possible to re-express Equation (4.110) as

$$\Omega_{\chi_0} = \frac{\pi}{3M_{Pl}^3 H_0^2 \langle\sigma v\rangle_{1,2}}\frac{g_*(T_0)}{g_*(T_\infty)}\sqrt{\frac{g_{eff}}{90}}x_f T_0^3. \tag{4.112}$$

Matter era and Dark Energy era

In the Matter era, the mass density $\rho_m(t)$ was grater than the radiation density $\rho_r(t)$, exactly the opposite to the Radiation era. In fact, Matter era begins when the radiation density decreases to the point when $\rho_r(t) = \rho_m(t)$ at some time t_{r-m} (i.e $\rho_r(t_{r-m}) = \rho_m(t_{r-m})$). The FLRW cosmological model predicts that the temperature at that time t_{r-m} was $T(t_{r-m}) = \dfrac{0.75eV}{k_B}$ [12].

The Dark energy era begins when the mass density decreases to the point when $\rho_m(t) = \rho_\Lambda(t)$ at some time $t_{m-\Lambda}$ (i.e $\rho_m(t_{m-\Lambda}) = \rho_\Lambda(t_{m-\Lambda})$). The FLRW cosmological model predicts that the temperature at that time $t_{m-\Lambda}$ was $T(t_{r-\lambda}) = \dfrac{0.33meV}{k_B}$ [12].

The values of $T(t_{r-m})$ and $T(t_{r-\Lambda})$ are lower than the temperature when the Freeze-Out occurs [13], i.e, in the Matter era and Dark Energy era $\Omega_\chi \approx \Omega_{\chi_0}$, turning these two epochs of the thermal history of the universe in something not very important to study the evolution of the density of DM.

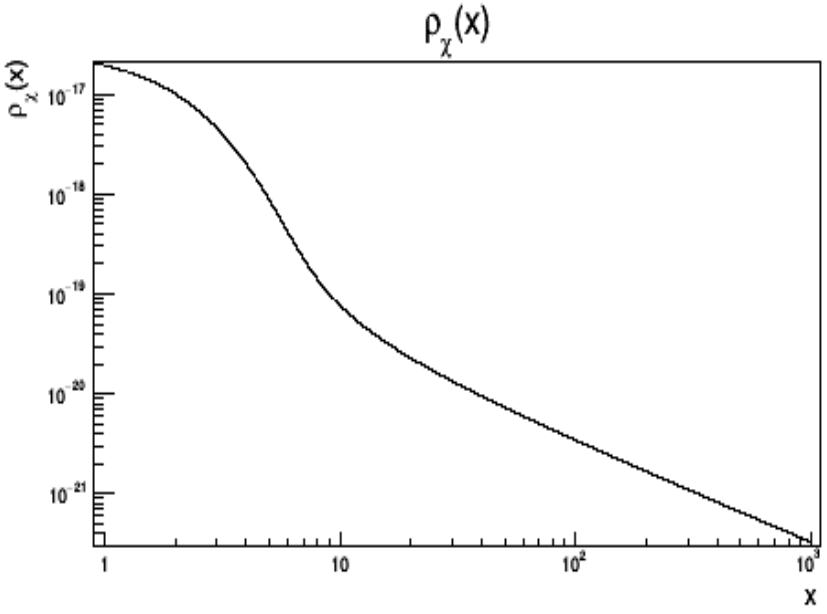

Figure 4.3: Illustration for ρ_χ vs x in the radiation era.

Chapter 5

SIMULATION OF THE COLLISION OF TWO CLOUDS OF DARK MATTER PARTICLES

5.1 Lattice Method

In the field of computer simulation for physic systems, the Lattice Method consist in the discretization of the phase-space for a system of particles that evolves in time. A special case of a Lattice Method is the Lattice-Boltzmann Method [14]. Because the resources of a computer are limited, some methods to perform many-bodies simulations with few resources are necessary, and Lattice Method is one of them. The space of velocities and positions are discretized in a finite number of boxes that forms a grid (or Lattice).

Every box in the grid is characterized by a function of the position and the velocity that dictates the probability of streaming of a particle in certain direction. For this simulation, there are three functions to describe the trajectory of a particle. First, a function that dictates the probability of scattering or annihilation in a collision of two particles. Second, another function that predicts the most probable position of a scattered particle, and third, a function that describes the free propagation of a particle.

Specifications of the Simulation

The simulation consists on apply the Lattice Method for a two dimensional space, with a grid of 300×300 boxes, to evolve in time a system of 10000 particles with interactions, divided in two spherical halos of 5000 particles each that will collide frontally. In the beginning of the simulation, every box in the Lattice is setted with some initial conditions that dictates the first step of the evolution of the system. The initial parameters that are set in the simulation are the initial velocity and position of each particle. The subsequent evolution of the system depends on the interactions between particles.

There are two types of interactions modeled in the simulation. The first interaction consist on direct contact between two particles. If two particles have the same position in the Lattice, then there is a probability of scattering and a probability of annihilation. The probability was chosen in such a way that it was proportional to the velocity-averaged cross section calculated for certain value of mass of the DM particle presented in Figure 5.1.

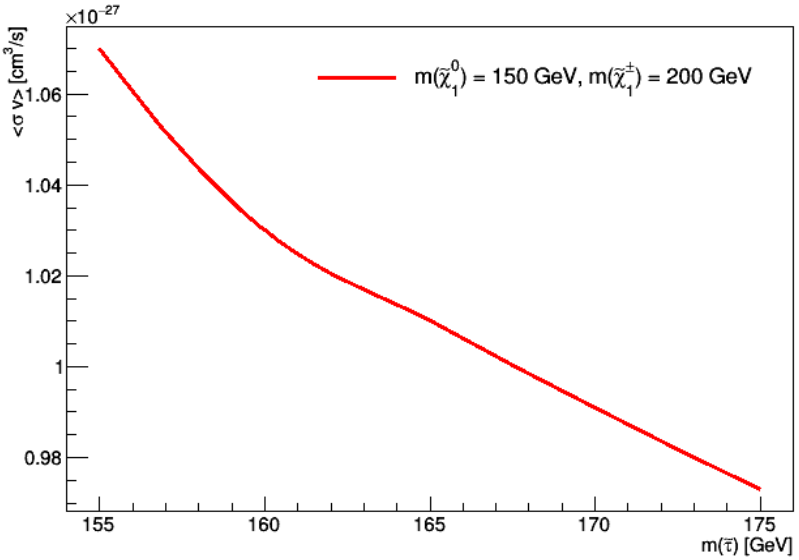

Figure 5.1: Illustration for $\langle \sigma v \rangle$ vs $m(\tilde{\tau})$ based in the minimal supersymmetric model

The minimal super-symmetric model, MSSM, was used to produce the curve in Figure 5.1. The conservation of the baryonic and leptonic quantum numbers in the decay of super-symmetric particles, referred to as R-parity conservation, was included in the model. Under this scenario, there a massive, stable, and neutral particle which naturally becomes a perfect DM candidate. This particle is referred to as the neutralino, $\tilde{\chi}_1^0$. The set of other super-symmetric parameters was chosen such that the resulting velocity-average cross-section gave a relic DM density consistent with that predicted from cosmological observations. Note that this implies a deep connection between particle physics and cosmology.

The velocities and positions of the particles after a scattering process were calculated with classical conservation of momentum and energy in a elastic collision. The fact that classical definitions were used to calculate velocities and positions implies that we are assuming a cold DM scenario, i.e a scenario where DM particles have a lower speed in comparison with the speed of light [15]. The second interaction is a contact interaction that includes the concept of a impact parameter. The velocities and positions of the DM particles after the collision via interaction with impact parameter are determined by classical mechanics, such as the scattering process in the description of the first interaction.

The simulation runs for 5000 iterations, where an iteration represents one unit of time. In this case, the standard unit of time (u.t) is 10^7 seconds, i.e each iteration represents 10^7 seconds in the simulation. The election of the unit of time is based in the fact that the radiation era is the period between 10^{-47} seconds to 30000 years after the big bang. In order to preserve the speeds of all particles lower than the 10% of the speed of light (the non-relativistic limit), each box represents an area of $10^{28}\,m$, but this definition could change in order to understand the simulation for different scales (Cosmological scales, Quantum scales, etc). For this case clearly a Cosmological scale was chosen.

5.2 Algorithm

The Algorithm of the simulation is described below. The first step is to set initial conditions for the system. Two circular clouds of particles are created with 5000 particles each cloud. The clouds are placed in opposite places, centered on certain specific points on the grid. By default the radius of each cloud is 60 boxes in the grid. The default positions in the grid for each cloud are 150 in vertical axis both and 75 and 225 in the horizontal axis for each cloud respectively. The initial disposition of the clouds is shown in Figure C.21. The initial magnitudes of velocities for each cloud by default are $1\,box/iteration$, the minimum possible non-zero velocity in the grid. This initial disposition of the system is printed in a .txt file called $0.png$.

The second step consists in evolving the system in time. In each iteration the frontier conditions are established. For this problem the frontier condition is periodic. Each particle moves, first, in a straight path in x axis in each iteration (in each unit of time) of the simulation. After the system evolves in time, the past positions and velocities of each particle are saved and actualized while three conditions are reviewed. The first condition to check is if a particle is in the same position in the x axes that another particle, but in a range of two boxes above or below. This condition is called *interaction via impact parameter*. If the condition is met, then a scattering process between the two particles that interact is considered.

The velocities for a scattering process in the horizontal axis (x axis) and the vertical axis (y axis) are calculated as follows. In an elastic collision of two particles the situation in Figure 5.2 is presented

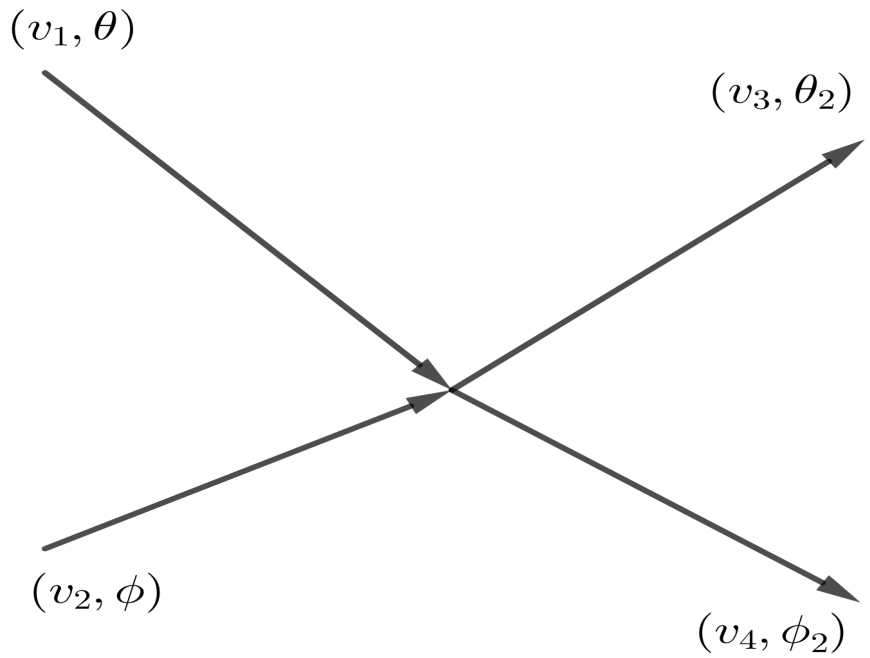

Figure 5.2: Vector diagram of moments for a elastic collision of two particles

The 2-tuples $(v_1, \theta), (v_2, \phi), (v_3, \theta_2)$ and (v_4, ϕ_2) represent the magnitudes and directions of the velocities of each particle involved in the collision process. In the process shown in Figure 5.2, two particles of DM (with the same mass) collide elastically. Equations (5.1) and (5.2) describe the conservation of momentum and energy for this process.

$$\begin{aligned} m\vec{v_1} + m\vec{v_2} &= m\vec{v_3} + m\vec{v_4} \\ \vec{v_1} + \vec{v_2} &= \vec{v_3} + \vec{v_4} \end{aligned} \tag{5.1}$$

$$\begin{aligned} \frac{1}{2}mv_1^2 + \frac{1}{2}mv_2^2 &= \frac{1}{2}mv_3^2 + \frac{1}{2}mv_4^2 \\ v_1^2 + v_2^2 &= v_3^2 + v_4^2 \end{aligned} \tag{5.2}$$

The vectors $\vec{v_1}, \vec{v_2}, \vec{v_3}$ and $\vec{v_4}$ are the velocity vectors shown in Figure 5.2. From the initial conditions of the simulation, the vectors $\vec{v_1}$ and $\vec{v_2}$ will always

be known. Directly from Equations (5.1) and (5.2) it is possible to obtain Equation (5.3)

$$\begin{aligned} \langle(\vec{v_1}+\vec{v_2}),(\vec{v_1}+\vec{v_2})\rangle &= \langle(\vec{v_3}+\vec{v_4}),(\vec{v_3}+\vec{v_4})\rangle \\ v_1^2+v_2^2+2\vec{v_1}\cdot\vec{v_2} &= v_3^2+v_4^2+2\vec{v_3}\cdot\vec{v_4} \\ \vec{v_1}\cdot\vec{v_2} &= \vec{v_3}\cdot\vec{v_4} \\ v_1v_2cos(\phi-\theta) &= v_3v_4cos(\theta_2-\phi_2), \end{aligned} \tag{5.3}$$

where $\langle\cdot,\cdot\rangle$ represents the inner product of two vectors. The system composed of Equations (5.1) and (5.2) is a system of three equations with four variables. To obtain an exact answer a four equation or constrain is needed. Assuming that $\phi-\theta=\theta_2-\phi_2$ as Equation (5.3) could suggest and choosing θ_2 to be a random value from 0 to 2π, it is possible to obtain from Equation (5.3) that

$$\begin{aligned} v_1v_2cos(\phi-\theta) &= v_3v_4cos(\theta_2-\phi_2) \\ v_1v_2 &= v_3v_4 \\ v_4 &= \frac{v_1v_2}{v_3} \end{aligned} \tag{5.4}$$

and, in consequence it is possible to obtain Equation (5.5) from Equation (5.2)

$$\begin{aligned} v_1^2+v_2^2 &= v_3^2+\left(\frac{v_1v_2}{v_3}\right)^2 \\ 0 &= v_3^4-(v_1^2+v_2^2)v_3^2+v_1^2v_2^2 \\ v_3 &= \pm\sqrt{\frac{(v_1^2+v_2^2)\pm\sqrt{(v_1^2+v_2^2)^2-4v_1^2v_2^2}}{2}}. \end{aligned} \tag{5.5}$$

To obtain a positive value for the magnitude v_3 in all cases, the positive roots are chosen and, in consequence the expression for v_3 change as shown in Equation (5.6).

$$v_3 = \sqrt{\frac{(v_1^2 + v_2^2) + \sqrt{(v_1^2 + v_2^2)^2 - 4v_1^2 v_2^2}}{2}}. \tag{5.6}$$

With all the arguments discussed above, it is possible to derive the solution set for the Equations (5.1) and (5.2). The solution set is composed of Equations (5.7), (5.8), (5.9)

$$v_3 = \sqrt{\frac{(v_1^2 + v_2^2) + \sqrt{(v_1^2 + v_2^2)^2 - 4v_1^2 v_2^2}}{2}} \tag{5.7}$$

$$v_4 = v_1 v_2 \left(\sqrt{\frac{(v_1^2 + v_2^2) + \sqrt{(v_1^2 + v_2^2)^2 - 4v_1^2 v_2^2}}{2}} \right)^{-1} \tag{5.8}$$

$$\phi_2 = \theta_2 + \theta - \phi. \tag{5.9}$$

The positions of the particles after the scattering are shown in Equation (5.10)

$$\begin{aligned} x_{n_1} &= x_{p_1} + \lceil v_3 cos\theta_2 \rceil \\ x_{n_2} &= x_{p_2} + \lceil v_4 cos\phi_2 \rceil \\ y_{n_1} &= y_{p_1} + \lceil v_3 sin\theta_2 \rceil \\ y_{n_2} &= y_{p_2} + \lceil v_4 sin\phi_2 \rceil \end{aligned} \tag{5.10}$$

where (x_{n_1}, y_{n_1}) and (x_{n_2}, y_{n_2}) are the positions of the particles after the scattering process and (x_{p_1}, y_{p_1}), (x_{p_2}, y_{p_2}) the positions of the particles before the collision and $\lceil x \rceil$ represent the ceil function of x.

The second condition to check is if two particles have the same position. If the condition is met, then a uniform random number is created. This random number have 10^{16} possible values between 0 and 1 and is the reference to choose between two cases. The first case happens if the random number is greater than certain value P. For this case a scattering process is considered in the same way it was previously treated. The second case happens if the

random number is lower than P. In this case the two particles that interact are annihilated. The value of P is conveniently chosen depending on what we want to analyze in the simulation.

After the two conditions were checked, then the number of particles in the grid are calculated and saved in a .txt file. The positions of all particles are saved in a .txt file too, named $k.txt$, where k refers to the number of iterations of the system ($0 \leq k \leq 5000$).

The third step of the simulation consists on graph the number of particles as a function of time and graph every $k.txt$ file in a .png file. All the .png files are converted in a .gif file to show more clearly the evolution of the system through time. For your interest, the Flux diagram for this algorithm are in **APPENDIX B**.

5.3 Implementation in C++

Each particle in the simulation is created, with all its characteristics, in a C++ class. The class that identifies each particle is called *Particula* and have the next characteristics.

Own variables of *Particula*

The particles described by *Particula* have 11 characteristic integer variables. The variables are described in the following list:

- *posac_i,posac_j*: These two variables describe the actual position of a particle in the x and y axes respectively.
- *pospas_i,pospas_j*: These two variables describe the past position (the position in a previous iteration of the simulation) of a particle in the x and y axes respectively.
- *velac_i,velac_j*: These two variables describe the actual velocity of a particle in the x and y axes respectively.

- *velpas_i,velpas_j*: These two variables describe the past velocity of a particle in the x and y axes respectively.

- *est*: This variable shows if the particle exist or not in the actual iteration of the simulation. The two values that this variable could take are 0 or 1.

- *estmov*: This variable helps to assign the path of each particle. Depending on the value of the variable, a function that change the state of movement of a particle will be called. The values that the variable could take are $1, 2, 3, 4, 5$ or 6.

- *activa*: This variable set the state of the particle if a collision happened. If the particle was annihilated *activa* take the value 0, in the opposite case, *activa* take the value 1.

Own functions of *Particula*

The function associated with a particle described by *Particula* and its descriptions are presented in the following list:

- *Particulapos(int,int),Particulavel(int,int)*: These two functions allows to set the positions and velocities of each particle. The function is used to define initial and frontier conditions.

- *evol1(),evol2(),evol3(),evol4(),evol5(),evol6()*: These functions change the path of a particle in certain cases. *evol1()* and *evol2()* are used to set the initial path of each halo, allowing that the two halos collide. After a horizontal collision of two particles, if the particles were scattered, *evol3()* and *evol4()* are used. In another case of scattering, functions *evol5()* and *evol6()* are used.

- *cambiarvelscat(int,int),cambiarvelcol(int,int)*: These two functions allow to change the velocities in the x and y coordinates of each particle, if a scattering process or collision process happened respectively.

- *estadoauno(),estadoacero()*: These two functions set the variable *est* to 1 or 0 respectively.

- *ann()*: Put the inactive particles out of the grid.

- *cambiarmov()*. The function allows to change the value of the variable *estmov*.

- *posaci(),posacj(),pospasi(),pospasj(),velaci(),velacj(),velpasi(),velpasj(), estado(),estadomov(),estadoact()*: These functions return the values of each of the 11 variables presented in the list of **Own variables** of *Particula*, respectively.

There are other auxiliary functions that do not belong to *Particula* but are useful for the simulation. The functions and their description are shown in the following list:

- *reset()*: Reset all the values of the grid to 0.

- *imprimir(int a)*: Allows to print the matrix that represents the grid in a file called *a.txt* (for different values of a).

- *imprimirn()*: Allows to print the array with the number of particles in each iteration in a file called *numero.txt*

- *random1(),random2()*: Allows to create the two circular halos, centered in a specific part of the grid and with certain radius.

- *arctang(int x, int y)*: Returns the value of the inverse tangent function of x/y.

- *asignarvelscat(int vel1x, int vel1y, int vel2x, int vel2y),asignarvelcol(int vel1x, int vel1y, int vel2x, int vel2y)*: Use Equations (5.7),(5.8) and (5.9) to calculate the velocity of two particles after an interaction.

After the definition of all functions, the main routine (called *Sim()*) is executed.

Graphing with Python

All the *k.txt* files, for $1 \leq k \leq 10000$ and *numero.txt* are loaded in a Python script called *graficas.py*. With the Python function *imshow()* all the *k.txt* are graphed, producing the files *k.png*. Another script in Python called *gifs.py* is used to join all the *k.png* in one file called *Simulacion.gif*.

All the *numero.txt* files produced for different values of the input parameters will be used for the analysis of the data obtained from the simulation in the next chapter.

Chapter 6

ANALYSIS OF THE DATA OBTAINED FROM THE SIMULATION

6.1 Physical Interpretation of the Data

As a reference to understand the results of the simulation, graphs of $N(t)$ vs t (number of particles in a time t vs time) are derived in order to understand the variation of the quantity $Y(t)$ that was treated in **Chapter 5**. If we know $N(t)$, also we could known the value of $Y(t)$ because $Y(t)$ is defined as in Equation (6.1)

$$Y(t) = \frac{N(t)}{(a(t)T(t))^3} \tag{6.1}$$

but, using Equation (4.61), Equation (6.1) becomes Equation (6.2)

$$N(t) = T_0^3 Y(t) \tag{6.2}$$

A measure of $Y(t)$ is a quasi-direct measure of $Y(t)$ for a system of particles and in consequence, a quasi-direct measure of the density of particles in the system.

With all the specifications named in past chapters, the simulation ran for different input parameters, such as the probability of annihilation, the

geometry of the particle clouds and the initial velocities of each cloud. Each case will be discussed below.

6.1.1 Different Probabilities of Annihilation

A set of probabilities was chosen to run the simulation in order to find a dependence with the number of particles in certain time. The initial velocities for each particle was chosen to be the minimum possible velocities, i.e the particle moves one position in the grid in one unit of time(one iteration). The shapes of the two clouds of DM were chosen to be circular with a radius of 60 boxes in the grid, as shown in Figure C.21. The results are shown in the dotted curves in Figures C.1,C.2,C.3,C.4 and C.5 in **APPENDIX C**. From Equation (4.102) is known that

$$\frac{\mathrm{d}Y}{\mathrm{d}x} \approx -\frac{m_\chi M_{Pl}}{\pi}\sqrt{\frac{90}{g_{eff}}}\,\langle\sigma v\rangle_{1,2}\,\frac{Y^2}{x^2} \tag{6.3}$$

but, in terms of the number of particles N, assuming that Equation (4.61) is true, and knowing that, for radiation era the FLRW model predicts that $a(t) = C_1\sqrt{t}$ with C_1 a constant [6], Equation (4.102) becomes Equation (6.4)

$$\frac{\mathrm{d}N}{\mathrm{d}t} = -C_2\frac{N^2}{t^{3/2}} \tag{6.4}$$

with $C_2 = \dfrac{k_B M_{Pl}}{2\pi c^2 T_0^2 C_1}\sqrt{\dfrac{90}{g_{eff}}}\,\langle\sigma v\rangle_{1,2}$. The solution of Equation (6.4) is

$$\begin{aligned} N &= \frac{\sqrt{t}}{\frac{\sqrt{t}}{N_\infty} - 2C_2} \\ (N - N_\infty)\sqrt{t} &= C_2 N_\infty N \end{aligned} \tag{6.5}$$

where $N_\infty = \lim_{t\to\infty} N(t)$.

Equation (6.5) says implicitly that the function that describes $N(t)$ correctly, in a physical sense is the one whose graphic of $(N-N_\infty)\sqrt{t}$ vs $N_\infty N$ is a

straight line with a slope of C_2 for large values of t. In Figures C.1,C.2,C.3,C.4 and C.5 $N(t)$ was fitted to an exponential function in order to describe $N(t)$ for great values of t and this exponential function is represented with a solid blue line. With this fitted function it is possible to graph $(N - N_\infty)\sqrt{t}$ vs $N_\infty N$.

In Figures C.6,C.7,C.8,C.9 and C.10 the graph of $(N - N_\infty)\sqrt{t}$ vs $N_\infty N$ is shown in a dotted line and the fit of the dotted line to a straight line is shown in a blue solid line. The fit of $(N - N_\infty)\sqrt{t}$ vs $N_\infty N$ to a straight line shows that the best model, according to physical principles, is the model that follows more exactly the shape of the fitted line. This model is the one where the probability of annihilation is 0.1.

With this probability, that we assumed proportional to $\langle \sigma v \rangle$ (in a factor of $1 \times 10^{-26}\, cm^3/s$ by simple observation of the order of magnitude of the velocity-averaged cross section) and the red curve showed in Figure 5.1, it is possible to find the mass of the candidate of DM particle that was treated in the simulation.

6.1.2 Different Shapes of the Clouds of Dark Matter

For this part, two cases were considered. The first is a collision of one circular cloud with a radius of 30 boxes an another cloud with a radius of 60 boxes in the grid. The second is a collision of two elliptical clouds, with the probability of collision was chosen to be 0.1, taking into account the results obtained in the previous subsection. The initial velocities were still fixed to be the minimum possible. An initial observation of the system for the first case is shown in Figure C.11 and for the second case is shown in Figure C.12.

For the first case, the graph of N vs. t is shown in Figure C.13 and its corresponding graph of $(N-N_\infty)\sqrt{t}$ vs $N_\infty N$ is shown in Figure C.14. The value of N_∞ predicted for this case is $N_\infty = 102$, a lower value in comparison to the obtained for the collision of two clouds with a radius of 60 boxes where N_∞ is approximately $1,8$ times higher. In this case the graph of $(N - N_\infty)\sqrt{t}$ vs $N_\infty N$ is not as similar to a straight line as in the case of Figure C.6, indicat-

ing that this case is not possible from the perspective of physics. The reason why this case is not a plausible option could be the short distance between particles in the cloud with a radius of 30 boxes. If an interaction via impact parameter is considered, this compressed cloud of particles can not keep its shape for a long time and it would disperse immediately, i.e, a structure like this should not exist in the universe, at least for an astronomical scale of time.

In the second case, the graph of N vs. t is shown in Figure C.15 and its corresponding graph of $(N - N_\infty)\sqrt{t}$ vs $N_\infty N$ is shown in Figure C.16. The value of N_∞ predicted for this case is $N_\infty = 92$ (it could vary because this is a simulation based in some aleatory variables), a lower value in comparison to the obtained for the collision of two clouds with a radius of 60 boxes where N_∞ is approximately 2 times higher. In this case, the graph of $(N - N_\infty)\sqrt{t}$ vs $N_\infty N$ is not as similar to a straight line as in the case of Figure C.6, indicating that this case is not possible from the perspective of physics, just like the first case. The reason why this case is not a plausible option could lie in the concept of isotropy. A cloud of massive particles composed only for one type of particle should take a spherical form (for this work, a circular form) in order to distribute its mass uniformly in space, not an perfect elliptical form.

6.1.3 Different Initial Velocities

The magnitude of the velocity of the particles in each cloud is changed, maintaining the probability of annihilation of 0.1 and the circular shapes of the two clouds, both with radius of 60 boxes in the grid. For the case when the magnitude of initial velocities are $1\,box/iteration$ and $10\,box/iteration$ for each cloud respectively, the graph of N vs t is shown in Figure C.17 and its corresponding graph of $(N - N_\infty)\sqrt{t}$ vs $N_\infty N$ is shown in Figure C.18. For another case when the magnitude of initial velocities are $150\,box/iteration$ for each cloud respectively, the graph of N vs t is shown in Figure C.19 and its corresponding graph of $(N - N_\infty)\sqrt{t}$ vs $N_\infty N$ is shown in Figure C.20.

For the cases mentioned above, the graphs of N vs t do not look similar to Figures C.1, C.13 and C.15. In this case is clear that those graphs do not

follow a physical behavior, but the reason why this happens lie in the discrete nature of the simulation. A great value for the magnitudes of initial velocities of each cloud of particles could lead to the fact that many interactions between particles that had to happen in a real system are ignored, making this simulation only good for small values of initial velocities.

6.2 Relation with Boltzmann Equation

The dotted lines in Figures C.1, C.13 and C.15 follow the same behavior of the solid blue line Figure 4.3 that shows the numerical solution for Boltzmann Equation (4.101), this means that the results of the simulation follow the physical behavior that Boltzmann Equation predicts for DM particles through time. The fact that the dotted line (black line) in Figure C.6 follows the behavior predicted in Equation (6.5) means that this simulation could reproduce all the physical concepts associated to the theory of the evolution of DM particles through time, discussed in **Chapter 4** and **Chapter 5**.

6.2.1 Dependence of N_∞ with the probability of annihilation

The simulation was used to predict the probability of annihilation of DM particles, but this simulation could work for modeling other particles, only changing the probability of annihilation (and in consequence the value of $\langle \sigma v \rangle$). The values of N_∞ as a function of the probability of annihilation for the collision of two circular clouds, both with radius of 60 boxes are shown in Figure 6.1

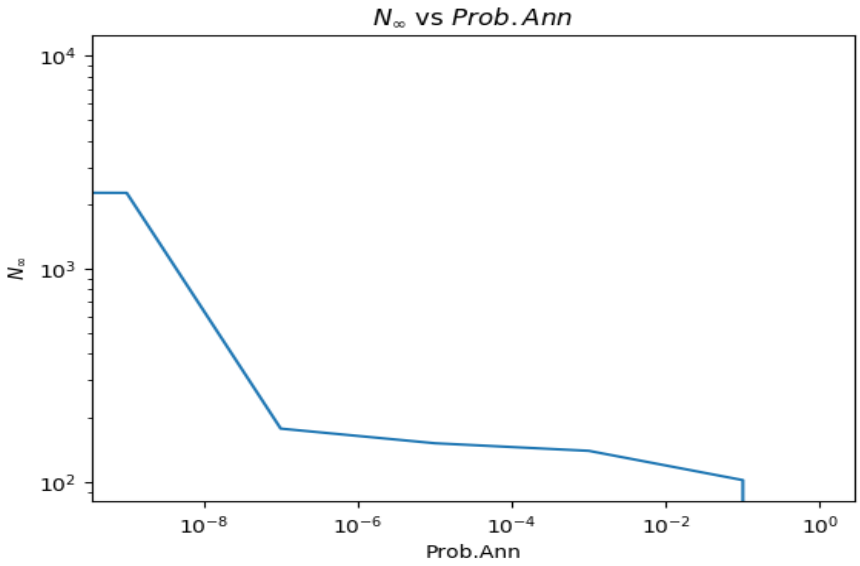

Figure 6.1: Illustration for N_∞ vs probability on annihilation.

6.3 Pros and Cons of the Simulation Method

Although the results of the simulation are in accordance with the theory that was discussed in **Chapter 4**, there are some aspects that the simulation does not allow to take into account. The Lattice simulation method allows to manage with discrete positions and velocities for each particle, making the processing of data much faster and effective and consuming less computational resources than other methods based in a continuous definitions for positions and velocities, however, the quantization of these quantities leads to the indirect quantization of the scattering angle, giving only a few possible trajectories for a particle after being scattered.

The method of discretization of the angles could be improved to take in count a larger range of possible angles and in consequence a larger number of possible trajectories for the particle, helping the simulation to become more isotropic, without a bias for the directions that each particle will take after an iteration [16].

6.4 Other Methods to Address the Problem

The analysis of the previous data was based in the Lattice method, described in **Chapter 5**, but there are other methods in which the simulation algorithm could be applied. One example of the methods named before is the N-bodies Simulation that will be described below.

6.4.1 N-bodies Simulation

A N-bodies Simulation is a way to determine the evolution in time of a N-bodies system. This method is used in theoretical studies of the large-scale structure of the Universe, climate modeling, microscopic dynamics among others. In a N-bodies simulation the initial velocities and positions of each body is defined, as well as the interaction forces between bodies. In each iteration of the simulation, the forces over a body are calculated to define its new velocities and positions. Mathematically a N-bodies simulation is defined by the solutions of a system of ordinary differential equations that describe the physical law present in the problem. For example, in a non relativistic gravitational N-bodies Simulation, the set of differential equations that dictate the behavior of the system comes from Newton's laws [17][18].

6.4.2 Pros and Cons of N-bodies Simulation

The N-bodies simulation, applied for the problem presented in this document, allows to have continuous values of velocities and positions, as well as non discretized values of scattering angle after a collision. Without a discrete value of the scattering value, each particle could have a greater number of possible trajectories after a collision and in consequence, the system will show a more isotropic behaviour, as would be expected from cosmological principles, nevertheless, the computational cost will increase compared to a Lattice Method.

Chapter 7

CONCLUSIONS

In the present work all the basic concepts about Dark Matter are explored and deepened. The astronomical point of view of Dark Matter is showed in order to introduce the point of view of particle physics. Some cosmological concepts derived from the FLRW model are developed from basic principles to understand all the details in the Boltzmann Equation and its solution, obtained by performing the Runge-Kutta Method of fourth order.

With the numerical solution of the Boltzmann Equation some approximations are considered in order to find an expression for the mass density of Dark Matter in the radiation era and to find the relic density of Dark Matter. The expression obtained for the relic density agrees with some previous results in [3].

In order to understand the concepts of annihilation probability and, in consequence, to understand the concept of annihilation cross section for DM particles, a computational simulation was performed. The simulation was based on the results shown in Figure 5.1, and it was aimed to study the behavior of a system of particles grouped in clouds and constrained to different values of input parameters, such as the probability of annihilation, the shape of the clouds and the initial velocity of each particle and constrained to two different interactions, one interaction via impact parameter and another via direct contact between particles. The Simulation shows that for a probability of annihilation of 0.1 the system reproduces the theoretical predictions of the Boltzmann Equation.

Although this work shows satisfactory results, according to the objectives, the topic, it is still under construction and will be improved in order to obtain more physical predictions derived from the simulation. As a next step to improve the present work, the system will be treated not in a 2D space but in a 3D space in order to reproduce a more realistic scenario. Another option to improve the work consists in interpolate the Cold Dark Matter scenario to a more general scenario where the velocities of the particles can be in the relativistic regime.

REFERENCES

[1] C. H. Lineweaver. "What is the Universe made of? How old is it?" In: *ArXiv Astrophysics e-prints* (Nov. 1999). eprint: astro-ph/9911294.

[2] E. Fischer. "The properties of dark matter". In: *ArXiv e-prints* (Mar. 2011). arXiv: 1104.2525 [physics.gen-ph].

[3] Juan Sanabria. "Búsquedas de Materia Oscura Supersimétrica en el LHC". In: *Revista de la Academia Colombiana de Ciencias Exactas, Físicas y Naturales* 38.0 (2014), pp. 34–55. ISSN: 2382-4980. DOI: 10.18257/raccefyn.153. URL: https://www.raccefyn.co/index.php/raccefyn/article/view/153.

[4] M. Lisanti. "Lectures on Dark Matter Physics". In: (2017). Ed. by J. Polchinski and et al., pp. 399–446. DOI: 10.1142/9789813149441_0007. arXiv: 1603.03797 [hep-ph].

[5] H. Goldstein, C.P. Poole, and J.L. Safko. "Classical Mechanics". In: (2002). URL: https://books.google.com.co/books?id=tJCuQgAACAAJ.

[6] C.W. Misner, K.S. Thorne, and J.A. Wheeler. *Gravitation*. Gravitation pt. 3. W. H. Freeman, 1973. ISBN: 9780716703440. URL: https://books.google.com.co/books?id=w4Gigq3tY1kC.

[7] G. van De Ven et al. "General solution of the Jeans equations for triaxial galaxies with separable potentials". In: *Monthly Notices of the Royal Astronomical Society* 342.4 (2003), pp. 1056–1082. DOI: 10.1046/j.1365-8711.2003.06501.x. eprint: /oup/backfile/content_public/journal/mnras/342/4/10.1046/j.1365-8711.2003.06501.x/2/342-4-1056.pdf. URL: http://dx.doi.org/10.1046/j.1365-8711.2003.06501.x.

[8] H.D. Young et al. *Sears and Zemansky's University Physics: With Modern Physics*. Addison-Wesley, 2012. ISBN: 9780321762184. URL: https://books.google.com.co/books?id=CCizKQEACAAJ.

[9] A. Zannoni. "On the Quantization of the Monoatomic Ideal Gas". In: *eprint arXiv:cond-mat/9912229* (Dec. 1999). eprint: cond-mat/9912229.

[10] T. Plehn. "Yet Another Introduction to Dark Matter". In: *ArXiv e-prints* (May 2017). arXiv: 1705.01987 [hep-ph].

[11] M. Lachièze-Rey. "Theoretical and Observational Cosmology". In: Nato Science Series C: (2012). URL: https://books.google.com.co/books?id=ThHvCAAAQBAJ.

[12] D. Baumann. "Thermal History". In: *Daniel D.Baumann 's University of Cambridge website* (). URL: http://www.damtp.cam.ac.uk/user/db275/Cosmology/Chapter3.pdf.

[13] S. Räsänen. "Thermal history of the early universe". In: *Syksy Räsänen 's lectures on cosmology* (). URL: http://www.courses.physics.helsinki.fi/teor/cos1/cosmo2015_05.pdf.

[14] S. Succi. *The Lattice Boltzmann Equation: For Fluid Dynamics and Beyond*. Numerical Mathematics and Scientific Computation. Clarendon Press, 2001. ISBN: 9780198503989. URL: https://books.google.com.co/books?id=0C0Sj%5C_xgnhAC.

[15] C. Armendariz-Picon and J. T. Neelakanta. "How cold is cold dark matter?" In: *jcap* 3, 049 (Mar. 2014), p. 049. DOI: 10.1088/1475-7516/2014/03/049. arXiv: 1309.6971.

[16] Antonio Fabio Di Rienzo et al. "Improved angular discretization and error analysis of the lattice Boltzmann method for solving radiative heat transfer in a participating medium". In: *International Journal of Numerical Methods for Heat & Fluid Flow* 21.5 (2011), pp. 640–662. DOI: 10.1108/09615531111135873. eprint: https://doi.org/10.1108/09615531111135873. URL: https://doi.org/10.1108/09615531111135873.

[17] *4 Gravitational Simulation*. URL: https://kof.zcu.cz/st/dis/schwarzmeier/gravitational_simulation.html.

[18] J. Adamek, R. Durrer, and M. Kunz. "Relativistic N-body simulations with massive neutrinos". In: 11, 004 (Nov. 2017), p. 004. DOI: 10.1088/1475-7516/2017/11/004. arXiv: 1707.06938.

Appendix A

APPENDIX A: General Relativity

A.1 General Relativity-FLRW metric

A.1.1 Definitions and conventions

Obtain $g^{\mu\nu}$ from the matrix representation of $g_{\mu\nu}$

If $g_{\mu\nu}$ is knowing, then $g^{\mu\nu}$ is defined by

$$g^{\mu\nu} = (g_{\mu\nu})^{-1} \tag{A.1}$$

where $(g_{\mu\nu})^{-1}$ is the inverse matrix of $g_{\mu\nu}$.

Obtain $g^{\mu\nu}$ from a diagonal matrix representation of $g_{\mu\nu}$

If $g_{\mu\nu}$ is of the form

$$g_{\mu\nu} = \begin{pmatrix} g_{00} & 0 & 0 & 0 \\ 0 & g_{11} & 0 & 0 \\ 0 & 0 & g_{22} & 0 \\ 0 & 0 & 0 & g_{33} \end{pmatrix} \tag{A.2}$$

then $g^{\mu\nu}$ is

$$g^{\mu\nu} = \begin{pmatrix} \frac{1}{g_{00}} & 0 & 0 & 0 \\ 0 & \frac{1}{g_{11}} & 0 & 0 \\ 0 & 0 & \frac{1}{g_{22}} & 0 \\ 0 & 0 & 0 & \frac{1}{g_{33}} \end{pmatrix} \tag{A.3}$$

As an annotation, if $g_{\mu\nu}$ is diagonal, then $g_{\mu\nu} = g_{\nu\mu}$

Einstein notation for repeated indices

If $A^{\mu\nu\dots}$ is a tensor and $B_{\mu\lambda\dots}$ is another tensor, then

$$A^{\mu\nu\dots}B_{\mu\lambda\dots} = A^{0\nu\dots}B_{0\lambda\dots} + A^{1\nu\dots}B_{1\lambda\dots} + A^{2\nu\dots}B_{2\lambda\dots} + A^{3\nu\dots}B_{3\lambda\dots} \tag{A.4}$$

Change of indices on a tensor

If $A^{\mu\nu}$ is a tensor of range 2 (with two indices), then the following relations are fulfilled:

$$\begin{aligned} g_{\nu\lambda}A^{\mu\nu} &= A^{\mu}_{\lambda} \\ g_{\sigma\mu}A^{\mu}_{\lambda} &= A_{\sigma\lambda} \\ g^{\kappa\sigma}A_{\sigma\lambda} &= A^{\kappa}_{\lambda} \\ g^{\lambda\gamma}A^{\kappa}_{\lambda} &= A^{\kappa\gamma} \end{aligned} \tag{A.5}$$

A.1.2 Properties of Christoffel symbols

For a diagonal metric tensor $g_{\mu\nu}$ the Christoffel symbols have the following properties

$$\begin{aligned} \Gamma^{\lambda}_{\mu\nu} &= 0 \qquad (\mu \neq \nu \neq \lambda) \\ \Gamma^{\mu}_{\mu\nu} &= \Gamma^{\mu}_{\nu\mu} = \frac{1}{2}\frac{1}{g_{\mu\mu}}\frac{\partial g_{\mu\mu}}{\partial x^{\nu}} \\ \Gamma^{\mu}_{\nu\nu} &= -\frac{1}{2}\frac{1}{g_{\mu\mu}}\frac{\partial g_{\nu\nu}}{\partial x^{\mu}} \\ \Gamma^{\mu}_{\mu\mu} &= \frac{1}{2}\frac{1}{g_{\mu\mu}}\frac{\partial g_{\mu\mu}}{\partial x^{\mu}}. \end{aligned} \tag{A.6}$$

As a clarification, it is necessary to explain that the term $\frac{1}{g^{\mu\mu}}$ is not "one over a matrix", but "one over the $g^{\mu\mu}$ component of the metric tensor $g_{\mu\nu}$".

A.1.3 Non-zero Christoffel symbols for FLRW metric

The non-zero Christoffel symbols for the FLRW metric are

$$\begin{aligned}
&\Gamma^0_{11} = \frac{a(t)\dot{a}(t)}{1-kr^2}, \Gamma^0_{22} = a(t)\dot{a}(t)r^2, \Gamma^0_{33} = a(t)\dot{a}(t)r^2\sin^2\theta, \\
&\Gamma^1_{11} = \frac{kr}{1-kr^2}, \Gamma^1_{22} = -r(1-kr^2), \Gamma^1_{33} = -r(1-kr^2)\sin^2\theta, \\
&\Gamma^2_{21} = \Gamma^2_{12} = \frac{1}{r}, \Gamma^2_{33} = -\sin\theta\cos\theta, \\
&\Gamma^3_{31} = \Gamma^3_{13} = \frac{1}{r}, \Gamma^3_{32} = \Gamma^3_{23} = \cot\theta, \\
&\Gamma^i_{i0} = \Gamma^i_{0i} = \frac{\dot{a}(t)}{a(t)} \qquad (i = 1, 2, 3).
\end{aligned} \tag{A.7}$$

Appendix B

APPENDIX B: Graphics in Chapter 5

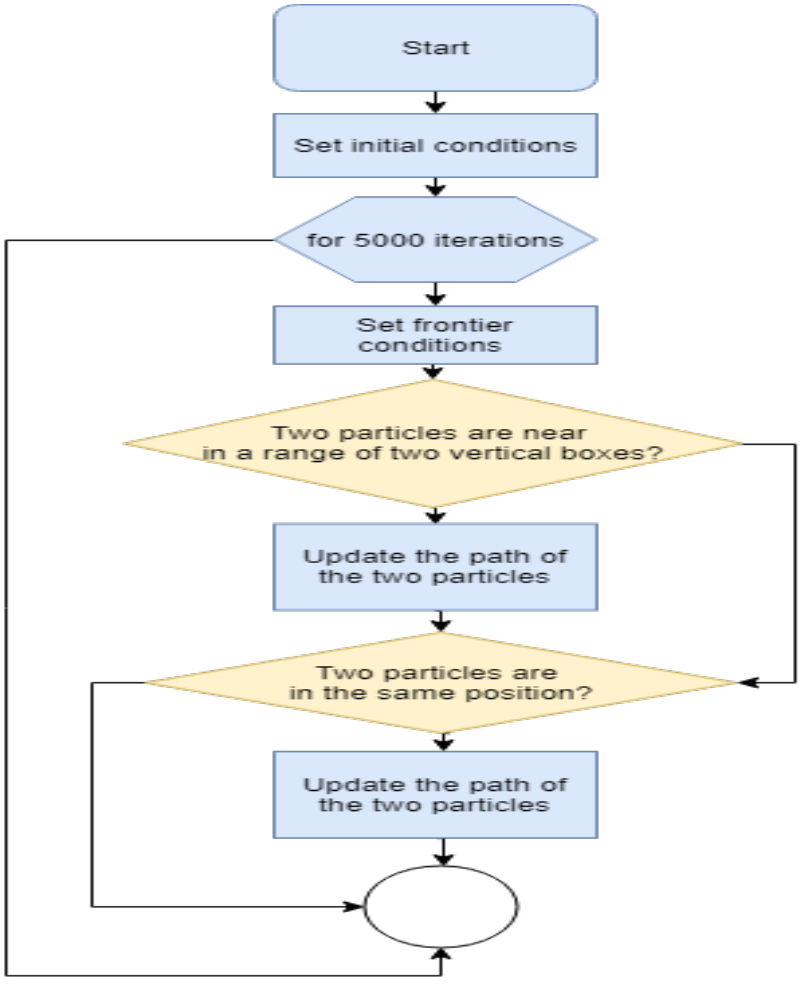

Figure B.1: Flux diagram for simulation

Appendix C

APPENDIX C: Graphics for Chapter 6

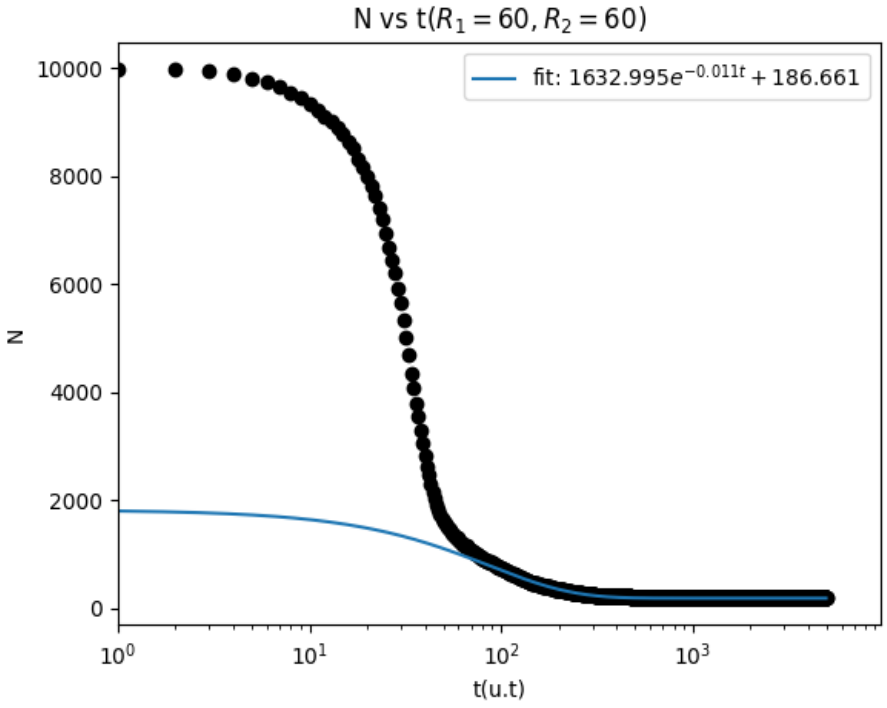

Figure C.1: Illustration for N vs t for a probability of annihilation of 10^{-1}.

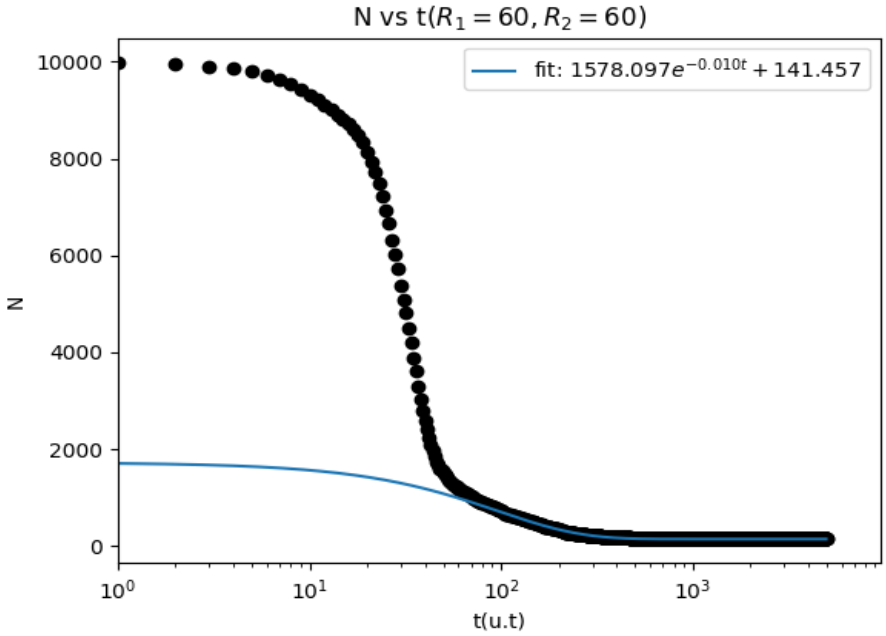

Figure C.2: Illustration for N vs t for a probability of annihilation of 10^{-3}.

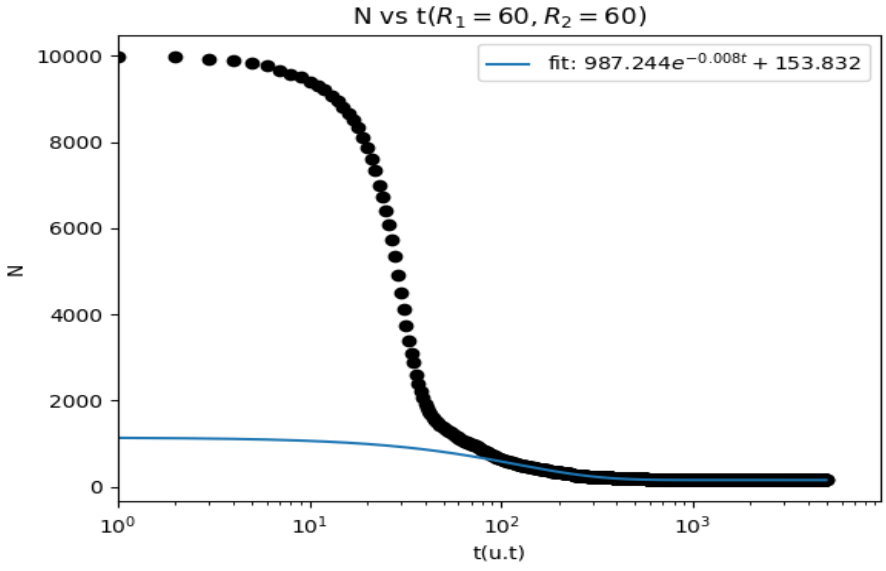

Figure C.3: Illustration for N vs t for a probability of annihilation of 10^{-5}.

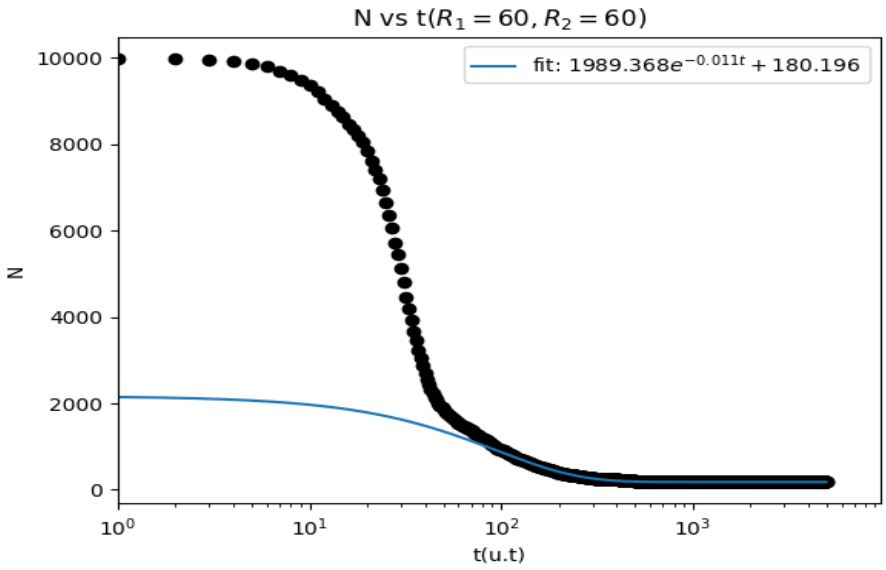

Figure C.4: Illustration for N vs t for a probability of annihilation of 10^{-7}.

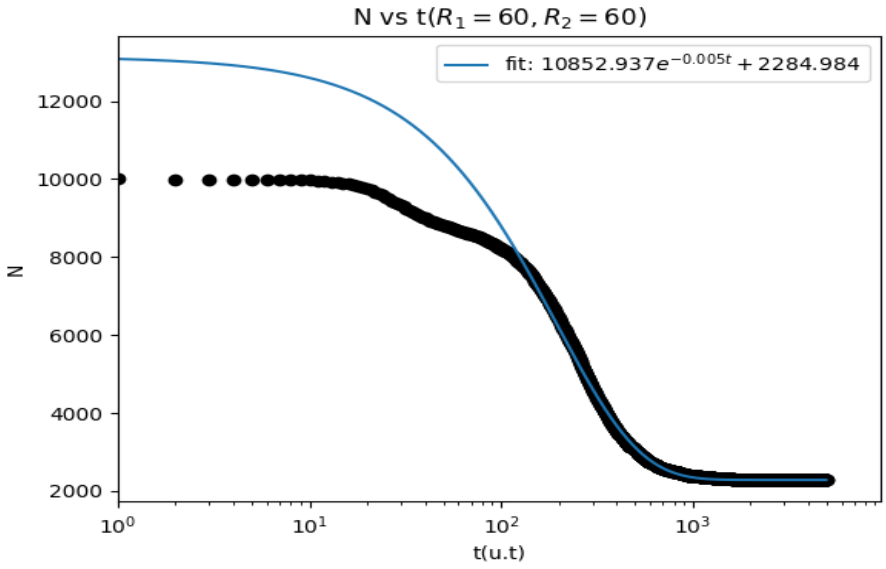

Figure C.5: Illustration for N vs t for a probability of annihilation of 10^{-9}.

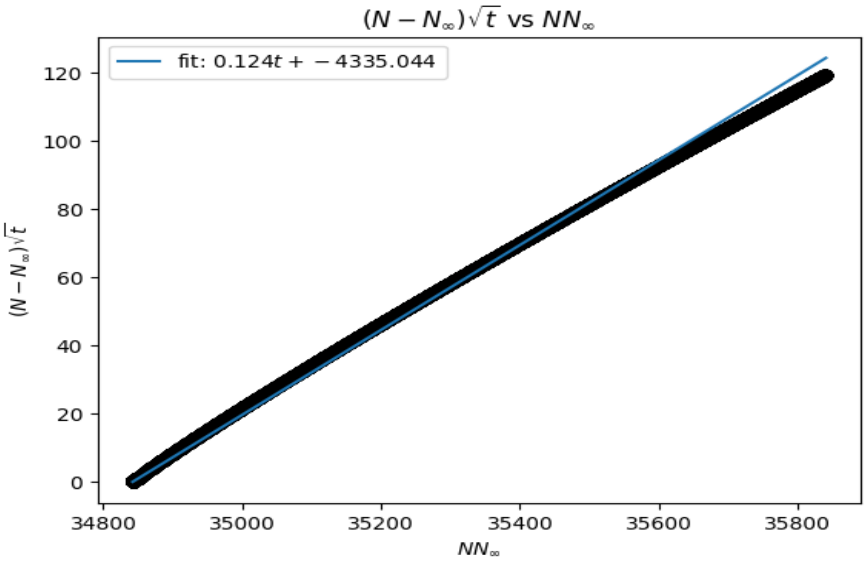

Figure C.6: Illustration for $(N - N_\infty)\sqrt{t}$ vs $N_\infty N$ for Figure C.1.

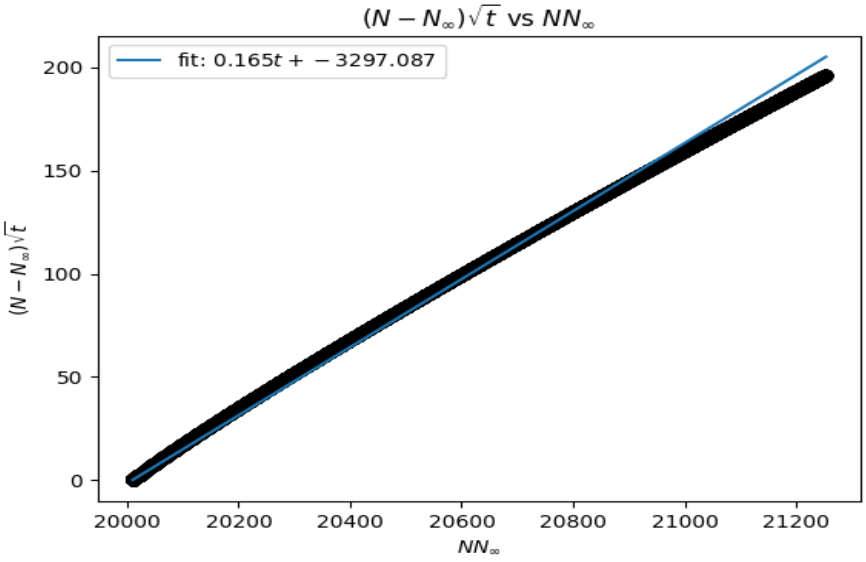

Figure C.7: Illustration for $(N - N_\infty)\sqrt{t}$ vs $N_\infty N$ for Figure C.2.

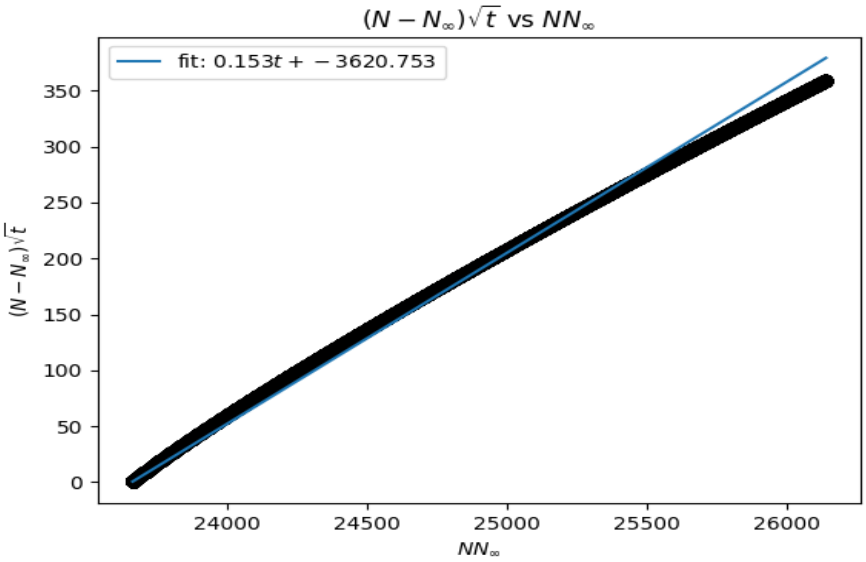

Figure C.8: Illustration for $(N - N_\infty)\sqrt{t}$ vs $N_\infty N$ for Figure C.3.

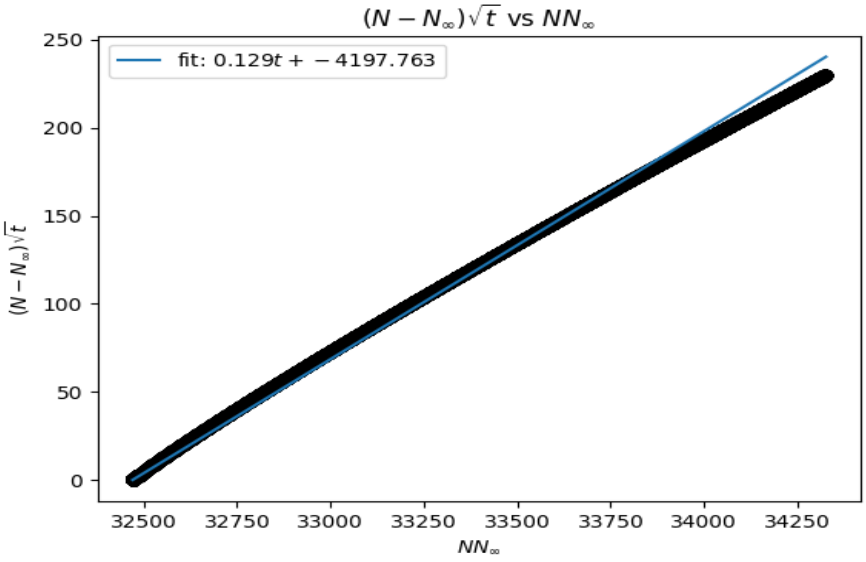

Figure C.9: Illustration for $(N - N_\infty)\sqrt{t}$ vs $N_\infty N$ for Figure C.4.

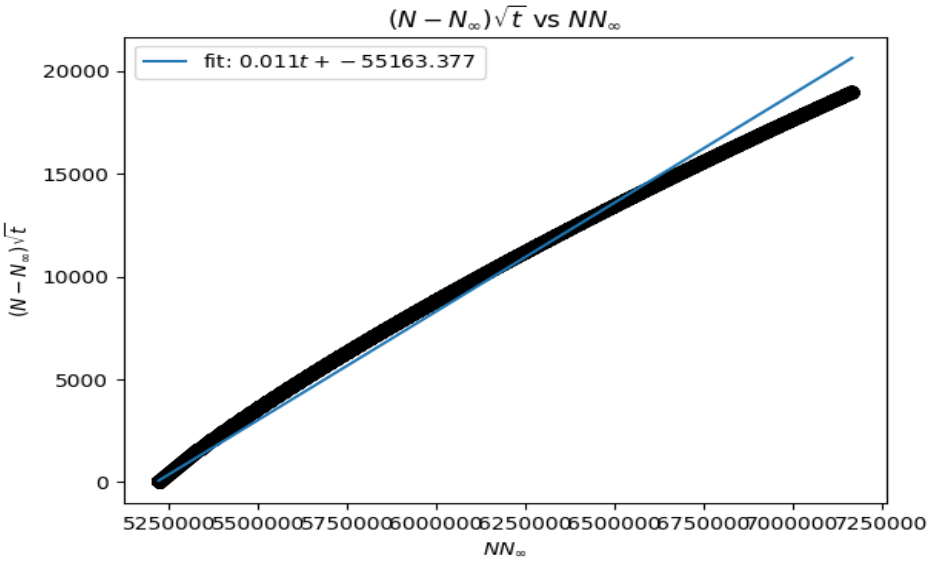

Figure C.10: Illustration for $(N - N_\infty)\sqrt{t}$ vs $N_\infty N$ for Figure C.5.

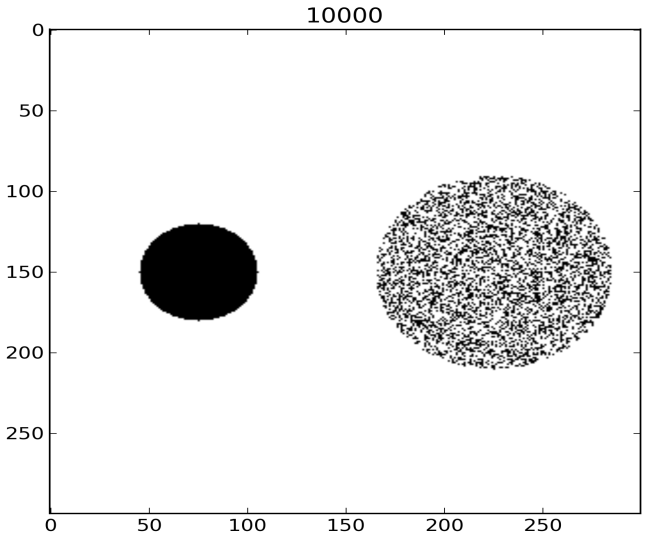

Figure C.11: Initial disposition of the system for two circular clouds of Dark Matter, one with radius of 30 boxes and another with radius of 60 boxes.

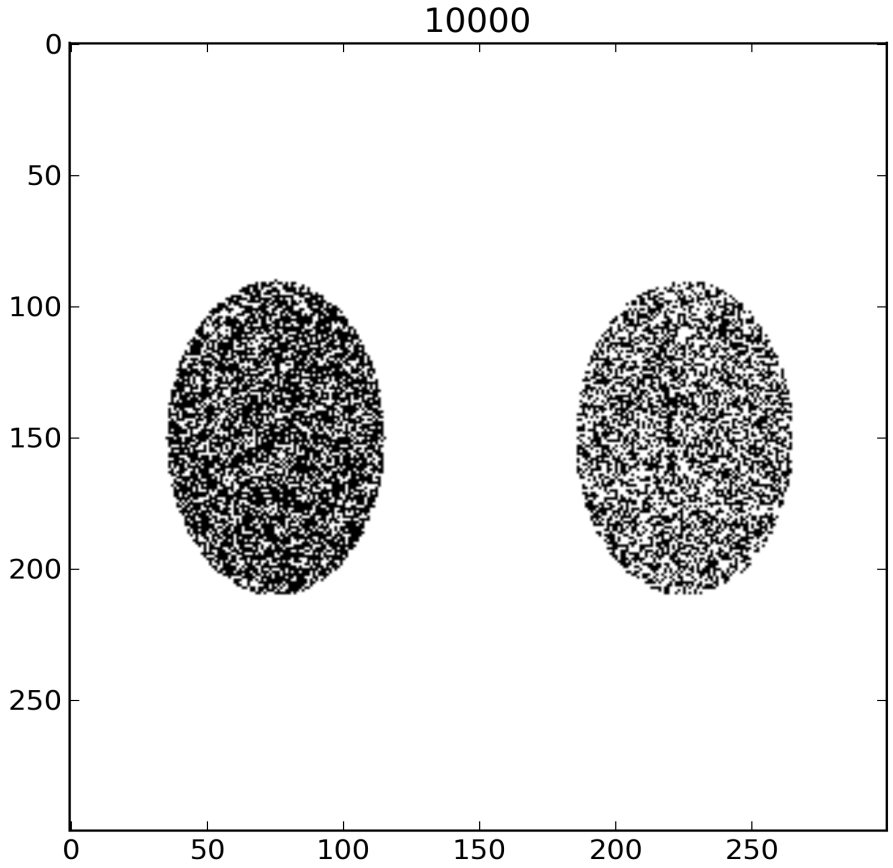

Figure C.12: Initial disposition of the system for two elliptical clouds of particles of Dark Matter with semi-major axis of 60 boxes in the vertical axis and semi-minor axis of 40 boxes in the horizontal axis

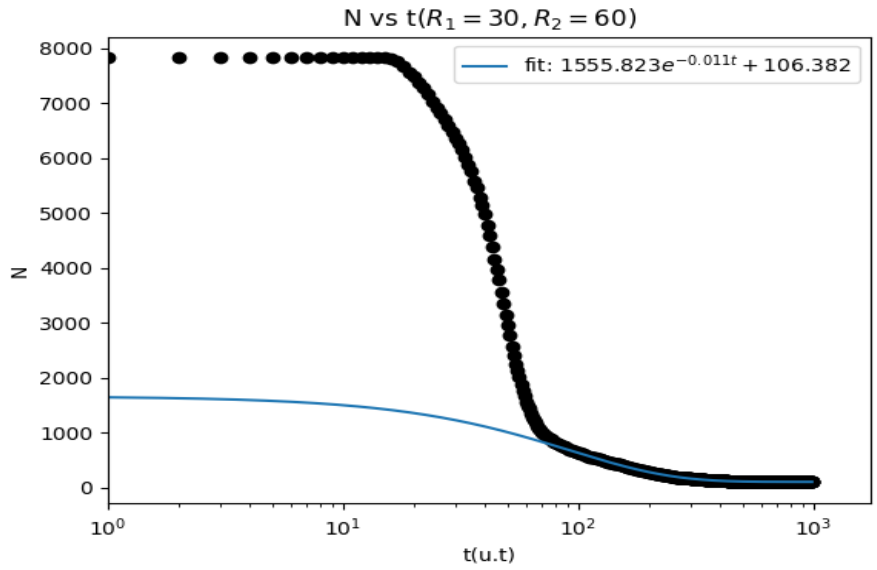

Figure C.13: Illustration for N vs t for the system of two circular clouds of Dark Matter, one with radius of 30 boxes and another with radius of 60 boxes.

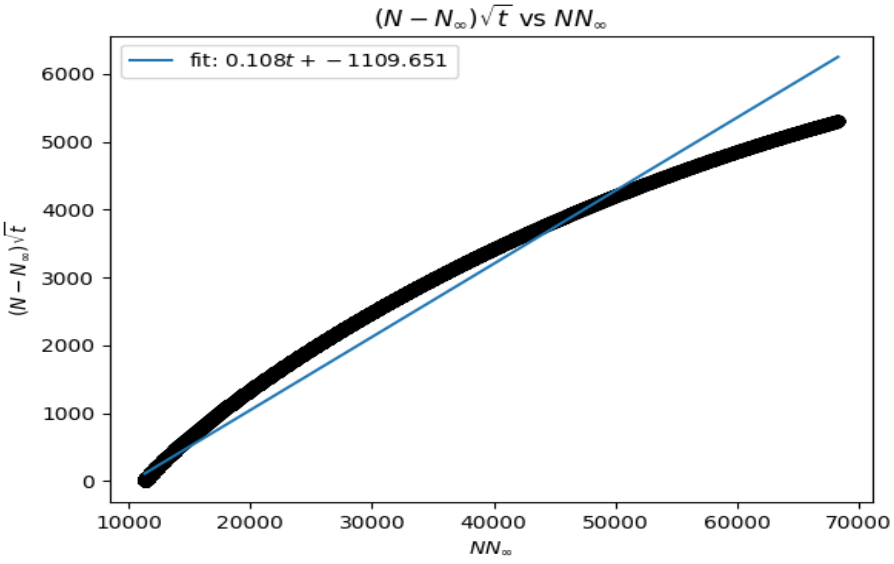

Figure C.14: Illustration for $(N - N_\infty)\sqrt{t}$ vs $N_\infty N$ for Figure C.13.

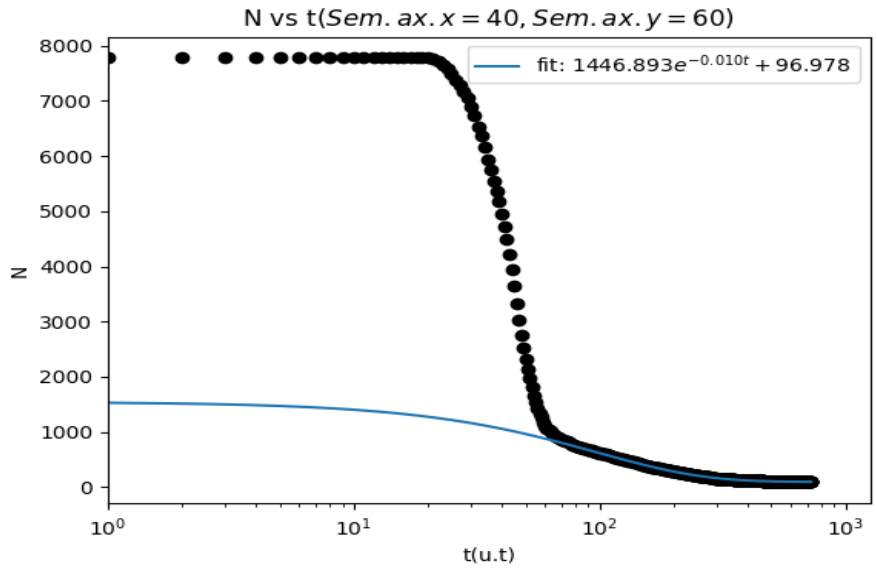

Figure C.15: Illustration for N vs t for the system of two elliptical clouds of Dark Matter, both with a semi-major axis of 60 boxes and a semi-minor axis of 40 boxes .

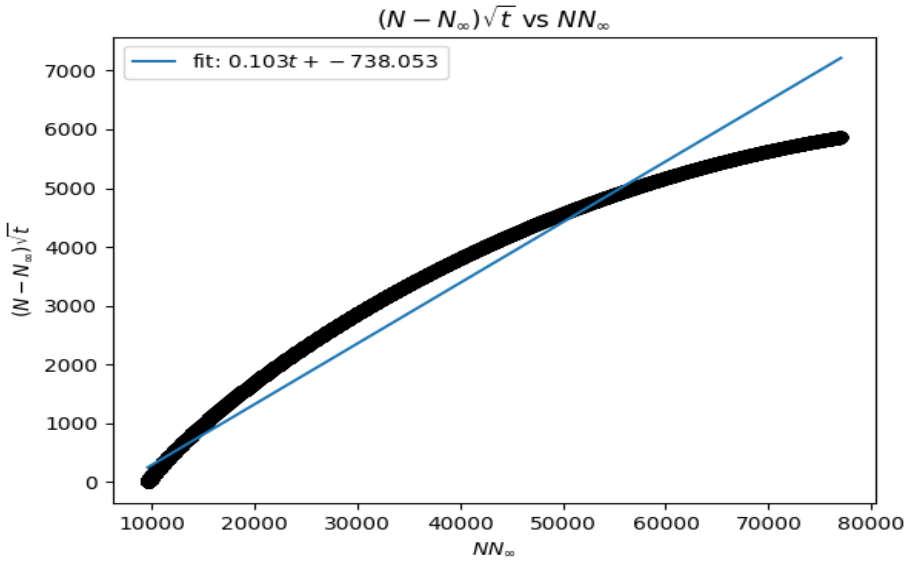

Figure C.16: Illustration for $(N - N_\infty)\sqrt{t}$ vs $N_\infty N$ for Figure C.15.

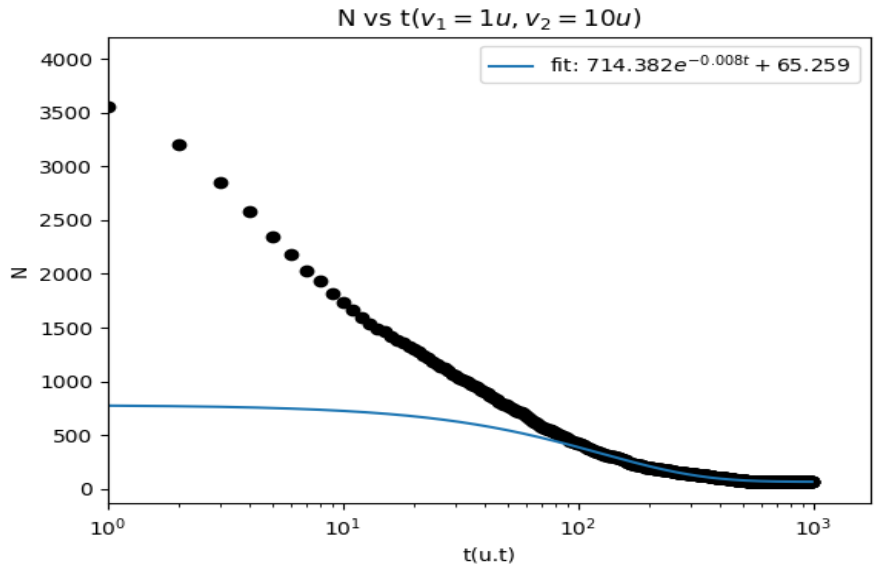

Figure C.17: Illustration for N vs t for initial magnitudes of velocities of $1\,box/iteration$ for one cloud and $10\,box/iteration$ for the other.

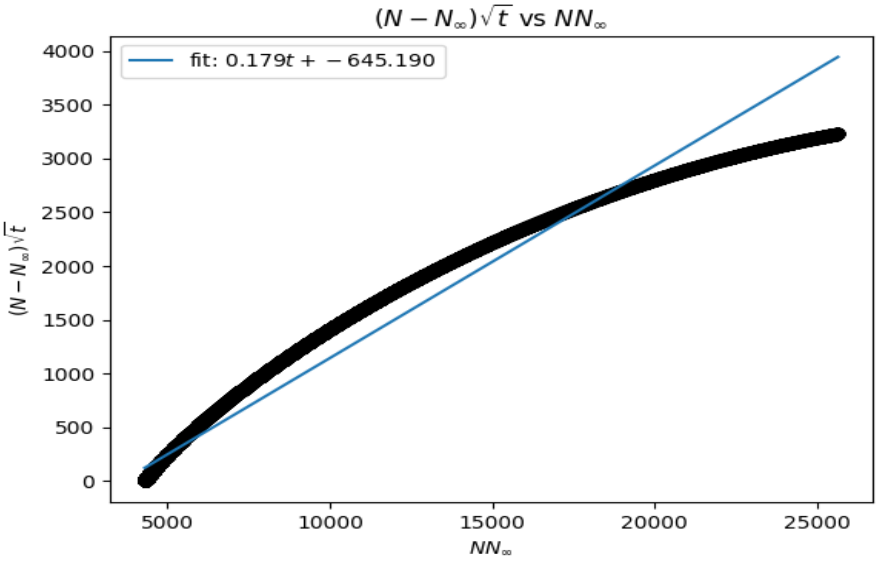

Figure C.18: Illustration for $(N - N_\infty)\sqrt{t}$ vs $N_\infty N$ for Figure C.17.

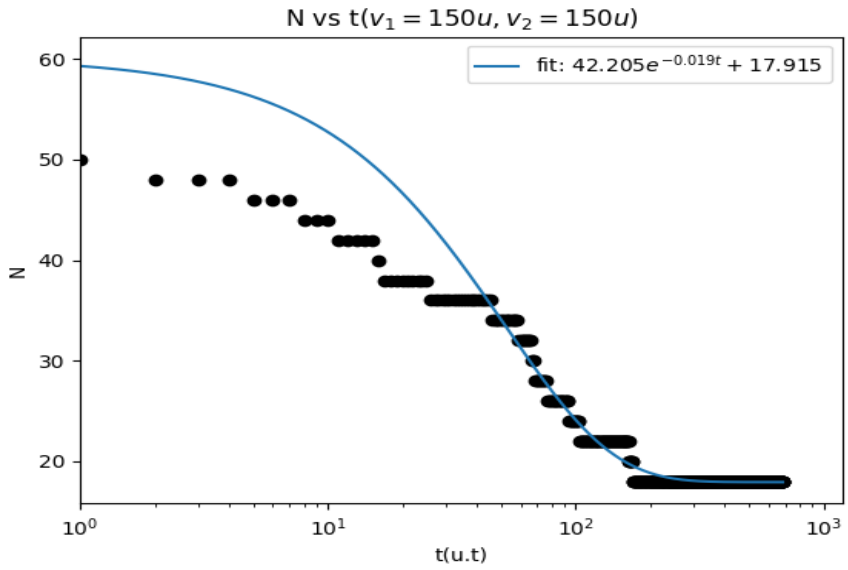

Figure C.19: Illustration for N vs t for initial magnitudes of velocities of $150\,box/iteration$ for one cloud and $150\,box/iteration$ for the other.

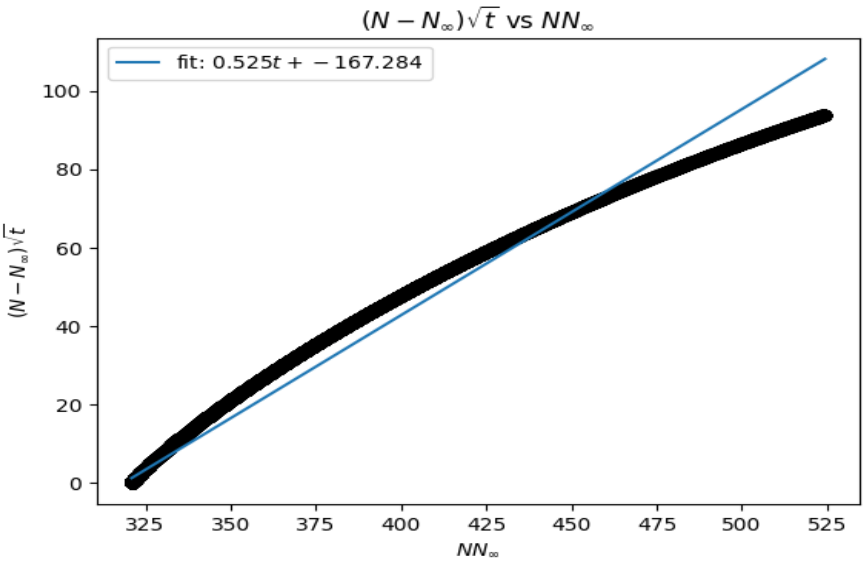

Figure C.20: Illustration for $(N - N_\infty)\sqrt{t}$ vs $N_\infty N$ for Figure C.19.

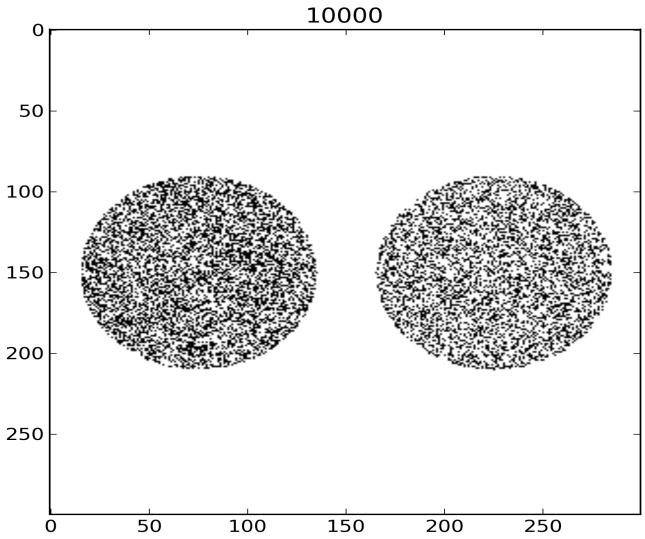

Figure C.21: Initial disposition of the system for two circular clouds of Dark Matter, both with radius of 60 boxes in the grid.